Modeling Radiative Transfer in Heterogeneous 3-D Vegetation Canopies

Jean-Philippe Gastellu-Etchegorry, Valérie Demarez, V. Pinel, F. Zagolski

ELSEVIER

Modeling Radiative Transfer in Heterogeneous 3-D Vegetation Canopies

J. P. Gastellu-Etchegorry, V. Demarez,* V. Pinel,* and F. Zagolski**

The DART (discrete anisotropic radiative transfer) model simulates radiative transfer in heterogeneous 3-D scenes that may comprise different landscape features; i.e., *leaves, grass, trunks, water, soil. The scene is divided into a rectangular cell matrix,* i.e., *building block for simulating larger scenes. Cells are parallelipipedic. Their optical properties are represented by individual scattering phase functions that are directly input into the model or are computed with optical and structural characteristics of elements within the cell. Radiation scattering and propagation are simulated with the exact kernel and discrete ordinate approaches; any set of discrete direction can be selected. In addition to topography and hot spot, leaf specular and first-order polarization mechanisms are modeled. Two major iterative steps are distinguished: 1) Cell illumination with direct sun radiation: Within cell multiple scattering is accurately simulated. 2) Interception and scattering of previously scattered radiation: Atmospheric radiation, possibly anisotropic, is input at this stage. Multiple scattering is stored as spherical harmonics expansions, for reducing computer memory constraints. The model iterates on step 2, for all cells, and stops with the energetic equilibrium. Two simple accelerating techniques can be used: 1) Gauss Seidel method,* i.e., *simulation of scattering with radiation already scattered at the iteration stage, and (2) decrease of the spherical harmonics expansion order with the iteration order. Moreover, convergence towards the energetic equilibrium is accelerated with an exponential fitting technique. This model predicts the bidirectional reflectance distribution function of 3-D canopies. Radiation components associated with leaf volume and surface mechanisms are distinguished. It gives also the radiation regime within canopies, for further determination of 3-D photosynthesis rates and primary production. Accurate modeling of multiple scattering within cells, combined with the fact that cells can have different x,y,z dimensions, is well adapted to remote sensing based studies,* i.e., *scenes with large dimensions. The model was successfully tested with homogeneous covers. Preliminary comparisons of simulated reflectance images with remotely acquired spectral images of a 3-D heterogeneous forest cover stressed the usefulness of the DART model for conducting studies with remotely acquired information.*

INTRODUCTION

Modeling the interaction of radiation with terrestrial surface is often a prerequisite for conducting research activities in several scientific domains. Two types of application of interest for environmental studies are mentioned here. The first deals with vegetation studies using remotely acquired information. In many cases, retrieving information from remotely sensed data would benefit of the use of three-dimensional (3-D) models that simulate accurately the spectral behavior of bidirectional reflectance distribution functions (BRDF) of Earth's surfaces. This is especially the case where it is intended to assess optical (e.g., albedo) and structural (e.g., leaf area index, LAI) characteristics of ground targets, or more generally where it is expected to associate signal characteristics (e.g., BRDF anisotropy) with some conditions of these targets. As an example, many studies already stressed the spectrally dependent anisotropic behavior of vegetation canopies (Kimes et al., 1986). Naturally, this is strongly influenced by the type of cover, the illumination configuration and the spectral domain. For example, Syren (1994) showed that for each degree of decreasing solar zenith angle nadir reflectance factors of pine and spruce forest covers increase by

*Centre d'Etude Spatiale de la Biosphère (UPS / CNRS / CNES), Toulouse, France

Address correspondence to J. P. Gastellu-Etchegorry, Centre d'Etude Spatiale de la Biosphère, CNES, CNRS-UPS, 18 Avenue Edouard Belin, Bpi 2801, 31401, Toulouse cdx, France.

Received 27 July 1995; revised 21 November 1995.

REMOTE SENS. ENVIRON. 58:131–156 (1996)

655 Avenue of the Americas, New York, NY 10010

0034-4257 / 96 / $15.00
SSDI 0034-4257(95)00253-7

1–2%, depending on the spectral domain, the tree species and the stand age. He observed most important increases with the young pines in the red (3%) and the near-infrared (2.5%) spectral regions. This confirms that in many cases the BRDF anisotropic behavior is a serious constraint for conducting vegetation studies with remote sensing data acquired under different experimental conditions, that is, viewing and illumination conditions. Associated errors depend on the target characteristics and the sun viewing conditions; for example, the albedo of a canopy with an anisotropic BRDF may be underestimated by as much as 45% if it is computed with nadir reflectance only (Kimes and Sellers, 1985). Moreover, the temporal variability of the anisotropy degree of vegetation BRDFs is an additional variable; however, provided that it may be determined with a sufficient accuracy, the latter is indicative of target conditions changes. Quantification of vegetation functioning is another important domain of application of radiative transfer models when these are coupled with leaf physiological models. Indeed, vegetation development is directly influenced by the within-stand radiation regime and the photosynthesis function of vegetation elements.

Various approaches have been developed in the past to model radiative transfer within canopies. They are based on mathematical formulation the complexity of which depends on their objectives, and include empirical functions (Walthall et al., 1985), semiempirical functions (Pinty and Ramond, 1986), simulation models with ray tracing, radiosity and Monte Carlo techniques (Borel et al., 1991; Jessel, 1992), geometric models (Li and Strahler, 1986), turbid models with the discrete ordinate method (Myneni et al., 1990; 1991), turbid models based on simplifications of the radiative transfer function (Gao, 1993), and turbid models with approximations of the radiative transfer function of Kubelka and Munk (Suits, 1972; Verhoef, 1984; Gastellu-Etchegorry et al., 1996). Depending on their complexity and on the type of available measurements (i.e., nadir, directional), these models are more or less convenient for retrieving pertinent information on land surfaces. Generally speaking, the spatial distribution of the target components is a major factor of the BRDF anisotropy. Its influence depends on the measurement configurations. Accurate modeling of canopy BRDF requires to take this factor into account.

Three-dimensional leaf canopy transport models such as the K-K model (Kimes and Kirchner, 1982; Kimes, 1991) provide an interesting means for taking into account the architecture of covers. The scene is divided into a rectangular cell matrix, and radiation transport is simulated with the discrete ordinate method; that is, source vectors are restricted to propagate in a finite number of directions. However, the K-K model presents some serious drawbacks (Myneni et al., 1991) due to simplifying assumptions. The most limiting weakness comes from the fact that multiple scattering processes that occur within cells are neglected. Moreover, propagation of cell scattered radiation is always simulated from cell centers. These simplifications lead to important errors whenever cells do not have infinitesimal optical depths. This is a very limiting constraint for remote sensing studies where the dimensions of cells must be large enough in order to allow one to work with large scenes. In this context, the hypothesis of cells with equal Cartesian dimensions is another weakness. Indeed, with large scenes the vertical dimension of cells is expected to be smaller than the horizontal cell dimensions; that is, a vertical length unit should be represented by a larger number of cells than the equivalent horizontal length unit. Another limitation arises from the hypothesis that discrete directions are equally spaced, which is far from optimal for accuracy and computer time purposes.

With these considerations in mind, we developed a new 3-D radiative transfer model (Gastellu-Etchegorry et al., 1994), hereafter called DART (Discrete Anisotropic Radiative Transfer) model. Similarly to the approaches of Kimes and Kirchner (1982) and Myneni et al. (1990), it is based on the discrete ordinate method and on an iterative approach. Moreover, the scene is a rectangular solid made of adjacent cells; that is, it is a cell matrix. The above-mentioned drawbacks are corrected. The 3-D radiation regime and the bidirectional reflectance distribution function (BRDF) of 3-D canopies are realistically simulated through the consideration of topography, major physical mechanisms such as the hot spot effect and leaf specular reflectance, and four types of scatterers (i.e., leaves and grass, soils, water, and trunks). Moreover, this model is aimed to allow one to distinguish the radiation components associated and not associated with leaf mesophyll information.

This article focuses on the mathematical description of the model. After a brief presentation of the scene modeling, the simulation of directional transport and the major steps of the iterative approach are described in the third section. This is followed by a full description of within cell scattering mechanisms. The emphasis is laid on single and multiple scattering mechanisms within leaf cells; scattering mechanisms that arise from other cell types are also described. Cell interactions are systematically analyzed by considering total scattered radiation, scattered radiation not associated with mesophyll information and first-order polarized scattered radiation. Two simple accelerating techniques for reducing computer memory constraints and computation times are described in the fifth section. Finally, a preliminary comparison between DART simulations and remotely acquired spectral images of a tree canopy is presented in the last section.

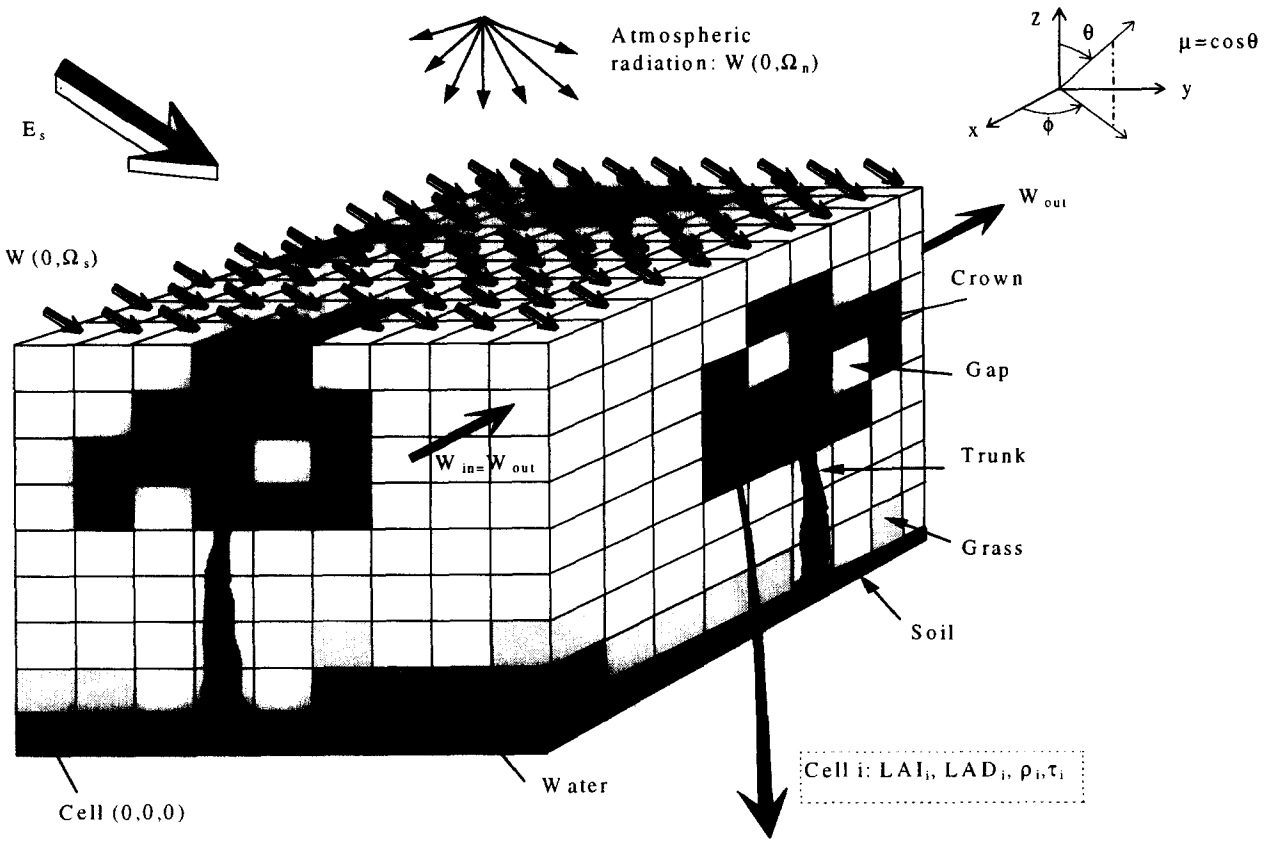

Figure 1. Representation of a cell matrix and its general illumination.

SCENE MODELING

The DART model does not require that the individual cells that constitute the 3-D scene have necessarily equal dimensions (Δx, Δy, Δz) along the *Ox*, *Oy*, and *Oz* axes. So, the numbers of cells along the vertical and horizontal axes can be independent, which results in important reductions in computer memory requirements and computation times. This is especially interesting for simulating the radiation regime of large scenes where the vertical variability is larger than the horizontal variability. Naturally, the selection of unequal dimensions along *Ox*, *Oy*, and *Oz* axes modifies the direction cosine values of the propagation directions.

Individual cells (Fig. 1) are identified with the *x*, *y*, and *z* coordinates of their centers. Lower (upper) cells of the scene have an altitude level $z = 0$ ($z = H$). The total number of cells is $I = (\Delta X \cdot \Delta Y \cdot \Delta Z) / (\Delta x \cdot \Delta y \cdot \Delta z)$, where ΔX, ΔY, and ΔZ are the Cartesian dimensions of the scene. Cells are used for simulating different types of scene elements, that is, leaves, soil surface, grass, water, and trunks. Depending on their information content, cells are simulated as turbid media, with volume interaction mechanisms, or solid media with surface and possibly volume interaction mechanisms. Cells characterized by different optical behaviors are said to belong to different types of cell. Two approaches can be used to specify the optical properties of each individual cell:

- Cell type *j*, with $j \in [1 \quad J]$, and specific optical and structural characteristics of the elements within the cell; for example, with leaf or grass cells, hereafter simply called leaf cells, these characteristics are the LAI, LAD (leaf angle distribution), and foliar reflectance and transmittance. In a first step, before tracking radiation propagation, the DART model uses these input parameters in order to compute the scattering transfer functions $T(j,\Omega,\Omega')$ that characterize cell volume scattering mechanisms of all *j* cell types; Ω and Ω' are the incident and scattered directions, respectively. Leaf transmission functions $T(j,\Omega)$ associated with a unit leaf area volume density and a unit propagation length are also computed for handling leaf cell interaction mechanisms.
- Cell type *j*, with $j \in [1 \quad J]$. This index indicates the relevant volume scattering transfer function $T(j,\Omega,\Omega')$. In the case of leaf cells, this index is input with the leaf cell area index. So, the index *j* indicates also the relevant cell transmis-

sion function $T(j,\Omega)$. These discretized functions may come from measurements, analytical computations or simulations conducted at finer spatial resolutions.

The information content of any cell is specific to that cell and is a constant for the whole cell. If necessary, the operator can easily add other types of elements, provided that he knows either their optical and structural characteristics or their transmission and scattering phase functions.

The K-K approach is adopted for dealing with scene boundary interactions. It is assumed that the whole scene can be considered as the juxtaposition of identical cell matrices. The hypothesis relies on symmetric considerations. So, the above-mentioned cell matrix is a simple building block that when replicated will simulate the entire scene. With the assumption that all neighbor cell matrices have identical optical behaviors, it results that as a source vector escapes the sides of the modeled cell matrix, there is an equivalent source vector escaping an adjacent cell matrix which enters the modeled cell matrix at a symmetric position. It means that the radiometric behavior of the entire scene can be simulated with the simulation of an individual cell matrix. The dimension of this cell matrix depends only on the basic unit of structural repetition within the scene; for example, it is smaller for homogeneous tree plantations than for disturbed dense forests (Kimes, 1991).

REPRESENTATION OF THE DIRECTIONAL TRANSPORT

Discretization of the Propagation Directions

The DART model relies on the discrete ordinate method; that is, the angular dependence in the transport equation is approximated by discretizing the angular variable Ω into a number N of discrete directions Ω_n, with $n \in [1 \quad N]$. These directions are the only possible directions of incident and scattered radiant fluxes. They are not necessarily equally spaced and can be selected *a priori* by the operator. The total number of discrete directions is

$$N = \sum_{u=1}^{U} \sum_{v=1}^{v(u)},$$

where u is the discretizing level of coordinate μ, that is the cosine of zenith angle θ, and v is the discretizing level of coordinate φ, that is, the azimuth angle. A negative μ indicates a downward direction, and a positive μ indicates an upward direction. Thus, for a zenith level u we have $v(u)$ azimuth levels. It means that the azimuth angles $\varphi(u,v)$ and $\varphi(u',v)$ may be different if the indices u and u' are different.

Discrete directions are associated with a number of contiguous sectors $\Delta\Omega_n$ defined by their azimuth $\Delta\varphi_n$ and zenith $\Delta\theta_n$ angle intervals. The solid angle of each sector is

$$\Delta\Omega_n = \int_{\Delta\varphi_n}\int_{\Delta\theta_n} |d\mu| \cdot d\varphi \qquad \text{with } \mu = \cos\theta$$

Moreover, we have

$$\sum_{n=1}^{N} \Delta\Omega_n = 4\pi \qquad \text{with } (\Omega_n) = (\theta_u, \varphi_v(\theta_u)).$$

The DART model starts with the determination of all cells encountered by any source vector that propagates in the scene 1) from the center of cell (0,0,0), and 2) from the center of each face of cell (0,0,0) for all N discrete directions (Ω_n). Indeed, geometric propagation of radiation is always simulated from cell centers or cell faces. This leads to the building up of seven look-up tables. For each cell i encountered the within cell propagation length Δl_i and the coordinates of the entrance point are systematically computed and stored for further processing. These look-up tables eliminate unnecessary repetitive computations during the tracking of source vectors. Thus, during the procedure that tracks radiation propagation, the coordinates of the ith cell encountered by a source vector that propagates within the scene are the coordinates of the cell where it originates plus the ith coordinates of the look-up table.

Radiation Transport

The general transfer equation of steady state monochromatic specific intensity $I(r,\Omega)$ at a position r and along a direction Ω (Hapke, 1993) is

$$\left[\mu \cdot \frac{d}{dz} + \eta \cdot \frac{d}{dy} + \xi \cdot \frac{d}{dx}\right] I(r,\Omega) =$$
$$-a(r,\Omega) \cdot I(r,\Omega) + \int_{4\pi} a_d(r,\Omega' \rightarrow \Omega) \cdot I(r,\Omega') \cdot d\Omega'. \quad (1)$$

μ, η, and ξ are directional cosines with respect to the z, y, and x axes, $a(r,\Omega)$ is the extinction coefficient, and $a_d(r,\Omega' \rightarrow \Omega)$ is the differential scattering coefficient for photon scattering from direction (Ω') into a unit solid angle about direction (Ω).

Assuming that we represent the N discrete directions by (Ω_n), with $n \in [1 \quad N]$, and that we distinguish the first and multiple collision terms, the angle discretized transport in 3-D Cartesian geometry along the (Ω_{ij}) direction is

$$\left[\mu_{ij} \cdot \frac{d}{dz} + \eta_{ij} \cdot \frac{d}{dy} + \xi_{ij} \cdot \frac{d}{dx}\right] I(r,\Omega_{ij}) =$$
$$-a(r,\Omega_{ij}) \cdot I(r,\Omega_{ij}) + Q(r,\Omega_{ij}) + \sum_{u=1}^{U} \sum_{v=1}^{v(u)} C_{uv} \cdot a_d(r,\Omega_{uv} \rightarrow \Omega_{ij}) \cdot I(r,\Omega_{uv}), \quad (2)$$

where u and v are the discretizing levels of coordinates μ and φ, respectively. Indices i and u belong to the interval $[1 \quad U]$, and indices j and v belong to the interval $[1 \quad v(u)]$. C_{uv} represents the weight associated with the

direction (Ω_{uv}) in the scattering mechanism ($\Omega_{uv} \rightarrow \Omega_{ij}$) where the incident radiation along the direction (Ω_{uv}) is scattered towards the direction (Ω_{ij}). $Q(r,\Omega_{ij})$ is the first collision source.

$I(r,\Omega_{uv})$ may represent either the mean specific intensity, that is,

$$\frac{1}{\Delta\Omega_{uv}} \cdot \int_{\Delta\Omega_{uv}} I(r,\Omega) \cdot d\Omega$$

in the angular sector $\Delta\Omega_{uv}$ or simply the exact specific intensity along the direction (Ω_{uv}). It depends on the definition of the differential scattering coefficients $a_d(r,\Omega_{uv} \rightarrow \Omega_{ij})$; that is, if they stand for mean values associated with scattering mechanisms from the angular sector $\Delta\Omega_{uv}$ towards the angular sector $\Delta\Omega_{ij}$, or if they stand for values associated with the scattering mechanism from direction Ω_{uv} towards direction Ω_{ij}. Of course, the values of weights C_{uv} differ depending on the meaning of the differential scattering coefficients. These weights must be chosen in order to satisfy symmetry and balance conditions (Myneni et al., 1991).

If $I(r,\Omega_{uv})$ and $a_d(r,\Omega' \rightarrow \Omega)$ are mean values, and provided that the angular sectors $\Delta\Omega_{uv}$ are sufficiently small and that the scattered radiation is not too anisotropic, then weights C_{uv} are simply assumed to be equal to $\Delta\Omega_{uv}$. On the other hand, if $I(r,\Omega_{uv})$ stands for the exact specific intensity along the direction (Ω_{uv}), the values of C_{uv} depend on the quadrature approach that is used to compute the integral of (1). In theory, the Gauss–Legendre quadrature is the most efficient approach. It leads to an approximation whose order is, essentially, twice that of Newton–Cotes formulas with the same number of evaluations of the specific intensity $I(r,\Omega_{ij})$. Naturally, high order of approximation is not the same as high accuracy. High-order translates to high accuracy only when the integrand is very smooth, in the sense of being well approximated by a polynomial (Press et al., 1992). Although the Gauss–Legendre quadrature approach is very general and simple, it has limitations. For example, with strongly anisotropic situations, it may be necessary to use an asymmetric set of Gauss–Legendre directions with several directions around the anisotropy or the anisotropies, which requires an *a priori* knowledge of the directional distribution of the anisotropies. A second and more serious weakness, called ray effect, arises in the case of 2-D and 3-D geometry. This is due to a defect in the discrete ordinates formulation itself. Indeed, according to the discretized radiative equations, scattered radiation can stream only along preset directions (Ω_n), which may imply that the influence of some isolated point sources, scatterers, and absorbers within the scene is totally ignored. The choice of equally spaced discrete directions tends to decrease the probability of ray effects. Finally, in the context of remote sensing studies, another limitation of the Gauss–Legendre quadrature originates from the fact that we usually require higher accuracy for directions close to the upward vertical (i.e., directions that are associated with viewing configurations from space) than for downward directions. As a result, it may be better to tailor an angular discretization scheme that is finer for upward directions close to the vertical.

In fact, as already mentioned, the DART model works with any input set of discrete directions (e.g., Gauss-Legendre directions or unevenly spaced directions). Functions that characterize cell interaction mechanisms, e.g., the scattering transfer functions and transmission functions of leaf cells, are determined with the so-called exact kernel method (Myneni et al., 1991). An example of computation of these functions is shown below in the following section. It follows that the discrete radiative transfer equation is simply:

$$\left[\mu_{ij} \cdot \frac{d}{dz} + \eta_{ij} \cdot \frac{d}{dy} + \xi_{ij} \cdot \frac{d}{dx}\right] W(r,\Omega_{ij}) = - a(r,\Omega_{ij}) \cdot W(r,\Omega_{ij}) + Q(r,\Omega_{ij}) \cdot \Delta\Omega_{ij} + \sum_{u=1}^{U} \sum_{v=1}^{v(u)} a_d(r,\Omega_{uv} \rightarrow \Omega_{ij}) \cdot \Delta\Omega_{ij} \cdot W(r,\Omega_{uv}), \quad (3)$$

where $W(r,\Omega_{uv})$ and $W(r,\Omega_{ij})$ are quantities that are proportional to the terms $I(r,\Omega_{uv}) \cdot \Delta\Omega_{uv}$ and $I(r,\Omega_{ij}) \cdot \Delta\Omega_{ij}$, respectively.

The physical quantity $W(r,\Omega_{uv})$ represents the flux of energy along the direction (Ω_{uv}) in a cone ($\Delta\Omega_{uv}$) at a position r. It can be envisioned as a flux of photons that stream through a cylinder of infinitesimal section ΔS ($\Delta S << \Delta x \cdot \Delta y$, $\Delta x \cdot \Delta z$ and $\Delta y \cdot \Delta z$) and the axis of which is parallel to the direction (Ω_{uv}). It has the dimension of a power (W).

$$W(r,\Omega_{uv}) = L_{\Delta S}(r,\Omega_{uv}) \cdot \Delta\Omega_{uv} \cdot \Delta S,$$

where $L_{\Delta S}(r,\Omega_{uv})$ is the radiance of the surface ΔS normal to the propagation direction (Ω_{uv}). We define the term "specific intensity associated with the flux $W(r,\Omega_{uv})$" with

$I(r,\Omega_{uv}) = \dfrac{W(r,\Omega_{uv})}{\Delta\Omega_{uv}}$ within a surface unit normal to the propagation direction (Ω_{uv}),

$I(r,\Omega_{uv}) = 0$ outside the above-mentioned surface unit.

Direct Sun Radiation and Anisotropic Atmosphere

The DART model was designed in order to handle both direct sun radiance and downward atmospheric radiance that may not be isotropic. Actually, the sky radiance distribution is often very anisotropic (Dave, 1978). Moreover, it ranges from 5% to 40% of the total downward radiance, under usual atmospheric conditions. Thus, total irradiance incident on a scene has two components: the direct sun and atmospheric source vectors. They are assumed to originate from a fictitious cell layer at the top of the scene. Direct sun source vectors (Fig.

1) propagate along the direction (Ωs). At the top of the scene their value is

$$W(\Omega_s) = E_s(\Omega_s) \cdot |\mu_s| \cdot \Delta x \cdot \Delta y,$$

and the atmospheric source vectors are

$$W_a(\Omega_n) = L_a(\Omega_n) \cdot |\mu_n| \cdot \Delta x \cdot \Delta y \cdot \Delta\Omega_n,$$

where $E_s(\Omega_s)$ is the sun constant at the top of the scene, Ω_s denotes the solar incident direction, and $L_a(\Omega_n)$ is the atmospheric specific intensity along direction (Ω_n), with $n \in [1 \quad N']$, where N' is the number of downward discrete directions. Anisotropic atmospheric conditions are simulated with the use of an anisotropic distribution $L_a(\Omega_n)$ that is specified by the operator. Different analytical expressions are available in the literature (Perraudeau, 1988). They depend on local sky conditions, that is, clear sky or cloudy sky. Three major approaches are generally followed for describing the angular distribution of the sky radiance (Liang and Stralher, 1993): 1) numerical solutions of the radiative transfer equation, 2) analytical approximations of the radiative equation, using for instance an Eddington-type approximation or a two stream approximation for the multiple scattering component, and 3) statistical techniques to fit collected sky radiance.

Thus, total downward irradiance of an upper cell is

$$\frac{1}{\Delta x \cdot \Delta y_n} \cdot \left[W(\Omega_s) + \sum_{n=1}^{N'} W_a(\Omega_n) \right].$$

Hereafter, a source vector, along direction (Ω_n) with $n \in [1 \quad N]$, incident on cell i, with $i \in [1 \quad I]$ is noted $W(0,\Omega_n)$. The associated transmitted source vector, after a propagation length Δl_i in cell i is noted $W(\Delta l_i, \Omega_n)$.

The Iterative Approach

The model processes the interactions of each individual source vector with all encountered cells as it propagates down and up in the scene (Fig. 2). During their propagation source vectors meet individual cells. Interaction mechanisms depend on the cell type, that is, the elements (leaves, soil, grass, water, trunk) within these cells and their associated structural and optical properties. Source vectors are transmitted through gaps, totally intercepted by opaque cells (e.g., soil and water cells), or partly intercepted and transmitted by semiopaque cells (e.g., trunk, leaf, and grass cells). Radiation intercepted by a cell gives rise to scattering and absorption mechanisms. Thus, each cell where scattering mechanisms take place becomes a secondary source.

In a first iteration all direct solar source vectors are processed. They give rise to secondary source vectors in all illuminated cells that are characterized by non-nil scattering phase functions. A solar source vector is processed until it reaches a zero threshold value T_1 or

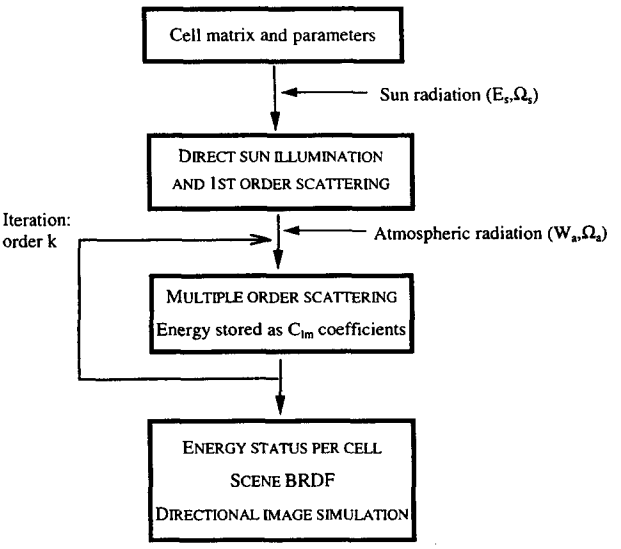

Figure 2. Schematic structure of the DART model.

encounters a medium where it is totally absorbed and scattered. This zero threshold value is selected by the operator; it is expected to be proportional to the incident irradiance multiplied by the relative error that is tolerated.

In a second iteration all source vectors that originate from all secondary sources, and the atmospheric source vectors, are processed. These give rise to tertiary source vectors that are further processed in a third iteration. Iterations are systematically conducted for all sources and for all N directions. Radiation that escapes from the upper cells of the scene is stored at each iteration. Processing goes on until source vectors escape from the canopy or reach a zero threshold level of flux within the scene. This threshold value is the product of an operator specified factor T_2 divided by 4π, and multiplied by the mean hemispherical flux $\langle \sum W \rangle_{1,2}$ and by the solid angle $\Delta\Omega_n$ of the cone of propagation. The term $\langle \sum W \rangle_{1,2}$ is the maximum value of the mean cumulated fluxes $\langle \sum W \rangle$ that exit cells in the first and second iterations. The quantities $\langle \sum W \rangle$ are computed during the illumination phases as the product of the cell single scattering albedos by the energy intercepted by the cells. Thus, $T_2 \cdot \langle \sum W \rangle_{1,2} / 4\pi$ is an intensity threshold. All source vectors $W(\Omega_n)$ that propagate across the scene such that

$$W(\Omega_n) < T_2 \cdot \langle \sum W \rangle_{1,2} \cdot \frac{\Delta\Omega_n}{4\pi}$$

are eliminated. Figure 3 shows the cumulated sums of cell scattered source vectors in iterations 1–8, in the case of an homogeneous foliar canopy (LAI = 2, spherical LAD, $\omega_{leaf} = 0.9$, $\rho_{soil} = 0$) with a direct sun illumination (SKYL = 0). The horizontal axis stands for the values of source vectors. All intensity values are divided by the

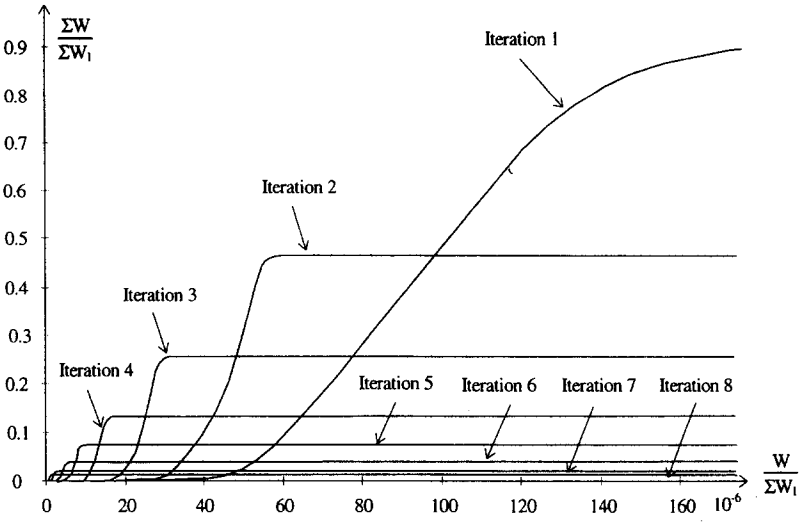

Figure 3. Cumulated sums of cell scattered source vectors in iterations 1–8 plotted against source vector intensity. Values are divided by the total energy scattered in the first iteration. They were obtained with an homogeneous leaf canopy (LAI = 2, spherical LAD, $\omega_{leaf} = 0.9$, $\rho_{soil} = 0$) and a direct sun illumination (SKYL = 0).

total energy scattered in the first iteration. Thus, the cumulated sum of the first iteration tends towards one, whereas asymptotic values in iterations 2–8 are 0.47, 0.25, 0.14, 0.07, 0.039, 0.021, and 0.011, respectively. The standard deviation of scattered source vectors strongly decreases with the iteration order; that is, the upper and lower cells tend to scatter the same energy at large iteration orders. Moreover, the larger intensity levels associated with iteration n tend to be systematically smaller than those associated with iteration orders smaller than n. So, the selection of a threshold intensity level equal to the mean source vector scattered at iteration n leads to the elimination of 1) all source vectors scattered at further iterations and 2) all source vectors that originate from iteration orders smaller or equal to n and that reach this threshold value after some propagation within the scene.

With clear sky conditions the intensity threshold value is selected with iteration one only because the mean scattered flux is larger for iteration 1 than for iteration 2. However, with very cloudy conditions, that is, conditions that are not appropriate for remote sensing acquisitions, this may not be true. This explains why iteration 2 is considered in addition of iteration 1. In that case, the model is not aimed to simulate remote sensing acquisitions but to simulate 3-D radiative transfer only, for example, for further modeling of canopy photosynthetic activity. The modulation of the threshold value by $\Delta\Omega_n$ is aimed to retain an acceptable accuracy along narrow anisotropic directions such as those associated with the hot spot configuration (i.e., equal illumination and viewing directions).

Scene Bidirectional Reflectance Factors

Once all source vectors have been processed, directional reflectance factors of all upper cells are computed. The energy flux that escapes an upper cell along direction (Ω_v) being $W_{out}(z = H,\Omega_v)$, the associated reflectance factor is

$$R(\Omega_v) = \frac{\pi \cdot W_{out}(z = H,\Omega_v)}{\mu_v \cdot \Delta\Omega_v} \cdot \frac{1}{W_s(z = H,\Omega_s) + \sum_{n=1}^{N} W_a(z = H,\Omega_n)}, \quad (4)$$

where

(Ω_v) = viewing direction with zenith and azimuth angles θ_v and φ_v,

$\mu_v = \cos\theta_v$,

$$\frac{1}{\Delta x \cdot \Delta y} \cdot \left[W_s(z = H,\Omega_s) + \sum_{n=1}^{N} W_a(z = H,\Omega_n) \right]$$

= total irradiance of an upper cell,

$$\frac{1}{\Delta x \cdot \Delta y} \cdot \frac{W_{out}(z = H,\Omega_v)}{\mu_v \cdot \Delta\Omega_v}$$

= radiance of an upper cell along the direction (Ω_v).

In the absence of atmospheric radiation, the upper cell bidirectional reflectance factor is

$$R(\Omega_s,\Omega_v) = \frac{\pi \cdot W_{out}(z = H,\Omega_v)}{W_s(z = H,\Omega_s) \cdot \mu_v \cdot \Delta\Omega_v}.$$

In a further stage the BRDF of each upper cell is resampled in a cylindrical coordinates system for obtaining a cylindrical representation of the BRDF. Depending on the choice of the operator, different types of results can be finally obtained. For example, if the position, viewing direction, and instantaneous field of view of the airborne or satellite sensor are known, the DART model simulates the remote acquisition of spectral images.

WITHIN CELL INTERACTIONS

When a source vector encounters a non empty cell, that is, a cell with some information content, the model handles interactions with the help of the cell optical

properties. Procedures used to simulate radiation interactions within cells depend directly on the cell type. For example, the simulation of scattering mechanisms within leaf cells relies on the use of scattering $T(j,\Omega,\Omega')$ and transmission $T(j,\Omega)$ functions, which is not the case with soil cells. As already mentioned, cell optical characteristics are either input parameters, or are computed in the first step of the DART simulation, with the optical and structural properties of the elements within the cell. An example of computation of leaf scattering and transmission functions is first examined. Handling other cells is globally similar. It is presented in a further section.

Leaf Cell Transmission

Leaf cells are treated as turbid media, with leaves assumed to be small plane surfaces with leaf scattering phase functions $f(j,\Omega_f,\Omega_s\rightarrow\Omega_v)$, where j indicates the cell type and (Ω_f) is the leaf normal orientation. The cell leaf area density is u_f. Leaf normals can have any possible orientation. They are defined independently of the N discrete directions of propagation. Their angular distribution is represented by the normalized leaf angle distribution function $g_f(j,\Omega_f)/2\pi$. Leaf cell dimensions must be such that enough leaf area is contained therein, upon which the use of local phytometric attributes such as $g_f(j,\Omega_f)$ would be meaningless. Natural vegetation clumping tends to ensure the validity of this hypothesis. Thus, the transmission factor (Fig. 3) associated with a radiation that propagates along a direction (Ω_n) through a foliar cell i of cell type j is

$$T(\Delta l_i,\Omega_n)=\exp[-G(j,\Omega_n)\cdot u_f(i)\cdot\Delta l_i],$$

where

$$G(j,\Omega_n)=\frac{1}{2\pi}\cdot\int_0^{2\pi}d\varphi_f\int_0^1 g_f(j,\Omega_f)\cdot|\Omega_n\cdot\Omega_f|\cdot d\mu_f$$

is the mean projection of a unit foliage area in cell i on a surface unit perpendicular to direction (Ω_n). Δl_i is the total pathlength through cell i along direction (Ω_n). We call $T(j,\Omega_n)$ the discretized $J\times N$ matrices $T(j,\Omega_n)=\exp[-G(j,\Omega_n)]$ with $j\in[1\quad J]$ and $n\in[1\quad N]$, where J' is the number of leaf cell types. Thus, we have

$$T(\Delta l_i,\Omega_n)=[T(j,\Omega_n)]^{u_f(i)\cdot\Delta l_i}.$$

Consequently, with a flux $W_{in}(0,\Omega_n)$ incident on cell i along the direction (Ω_n) the transmitted flux that escapes cell i along the direction (Ω_n) is

$$W_{out}(\Delta l_i,\Omega_n)=T(\Delta l_i,\Omega_n)\cdot W_{in}(0,\Omega_n). \tag{5}$$

It results that the source vector intercepted along the path $(\Delta l_i,\Omega_n)$ is

$$W_{int}(\Delta l_i,\Omega_n)=[1-T(\Delta l_i,\Omega_n)]\cdot W_{in}(0,\Omega_n). \tag{6}$$

Scattering Transfer Functions of Leaf Cells

The propagation (Fig. 4) of a source vector $W(l,\Omega_s)$ throughout a cell i along a direction Ω_s, where $l\in[0,\ \Delta l_i]$ is the pathlength from the entrance point (A) of cell i, gives rise to scattered source vectors $\mathscr{W}_1(\Delta l_i,\Omega_s\rightarrow\Omega_v)$ along the directions $(\Omega_v,\ \Delta\Omega_v)$, $v\in[1\ \mathrm{N}]$. The type of cell i being j, we have

$$\mathscr{W}_1(\Delta l_i,\Omega_s\rightarrow\Omega_v)=\int_{\Delta\Omega_v}\int_{\Delta l_i}\int_{2\pi}W(l,\Omega_s)\cdot u_f(i)\cdot|\Omega_s\cdot\Omega_f|\cdot\frac{g_f(j,\Omega_f)}{2\pi}$$

$$\cdot f(j,\Omega_f,\Omega_s\rightarrow\Omega_v)\cdot d\Omega_f\cdot dl\cdot d\Omega_v=W_{in}(0,\Omega_s)\cdot\frac{[1-T(\Delta l_i,\Omega_s)]}{G(j,\Omega_s)}$$

$$\cdot\int_{\Delta\Omega_v}\int_{2\pi}|\Omega_s\cdot\Omega_f|\cdot\frac{g_f(j,\Omega_f)}{2\pi}\cdot f(j,\Omega_f,\Omega_s\rightarrow\Omega_v)\cdot d\Omega_f\cdot d\Omega_v$$

$$=\frac{W_{int}(\Delta l_i,\Omega_s)}{G(j,\Omega_s)}\cdot\int_{\Delta\Omega_v}\int_{2\pi}|\Omega_s\cdot\Omega_f|\frac{g_f(j,\Omega_f)}{2\pi}$$

$$\cdot f(j,\Omega_f,\Omega_s\rightarrow\Omega_v)\cdot d\Omega_f\cdot d\Omega_v,$$

where $f(j,\Omega_s\rightarrow\Omega_v,\Omega_f)$ is the leaf scattering phase function.

The total specific intensity $\mathscr{I}(\Delta l_i,\Omega_s\rightarrow\Omega_v)$ associated with the flux $\mathscr{W}_1(\Delta l_i,\Omega_s\rightarrow\Omega_v)$ is

$$\mathscr{I}_1(\Delta l_i,\Omega_s\rightarrow\Omega_v)=I(0,\Omega_s)\cdot\Delta\Omega_s\cdot\frac{[1-T(\Delta l_i,\Omega_s)]}{G(j,\Omega_s)}$$

$$\cdot\int_{2\pi}|\Omega_s\cdot\Omega_f|\cdot\frac{g_f(j,\Omega_f)}{2\pi}\cdot f(j,\Omega_f,\Omega_s\rightarrow\Omega_v)\cdot d\Omega_f.$$

With small angular sectors the cumulated scattered flux to direction Ω_v is

$$\mathscr{W}_1(\Delta l_i,\Omega_s\rightarrow\Omega_v)=\frac{W_{int}(\Delta l_i,\Omega_s)}{G(j,\Omega_s)}\cdot\int_{2\pi}|\Omega_s\cdot\Omega_f|\cdot\frac{g_f(j,\Omega_f)}{2\pi}$$

$$\cdot f(j,\Omega_f,\Omega_s\rightarrow\Omega_v)\cdot d\Omega_f\cdot\Delta\omega_v,$$

$$\mathscr{W}_1(\Delta l_i,\Omega_s\rightarrow\Omega_v)=W_{in}(0,\Omega_s)\cdot[1-T(\Delta l_i,\Omega_s)]\cdot T(j,\Omega_s,\Omega_v), \tag{7}$$

where $W_{in}\ (0,\Omega_n)$ is the value of the source vector, along direction (Ω_s), at the entrance of cell i, and $T\ (j,\Omega_s,\Omega_v)$ is the cell transfer function. This is discretized as a $N\times N$ scattering transfer matrix the terms of which are equal to

$$[T(j,\Omega_s,\Omega_v)]=\int_{\Delta\Omega_v}\frac{\int_{2\pi}\frac{g_f(j,\Omega_f)}{2\pi}\cdot|\Omega_s\cdot\Omega_f|\cdot f(j,\Omega_f,\Omega_s\rightarrow\Omega_v)\cdot d\Omega_f}{G(j,\Omega_s)}\cdot d\Omega_v$$

Scattering transfer matrices $[T(j,\Omega_s,\Omega_v)]$ are precomputed in order to minimize repetitive computations. Each scattering transfer matrix $[T(j,\Omega_s,\Omega_v)]$ is broken up into two matrices that are assumed to be dependent $[T_d(j,\Omega_s,\Omega_v)]$ and independent $[T_s,(j,\Omega_s,\Omega_v)]$ of leaf mesophyll information. These scattering transfer matrices may be anisotropic and rotationally variant. They can be derived from radiometric measurements or from computations based on whatever method is selected; for example, with the usual assumption under which

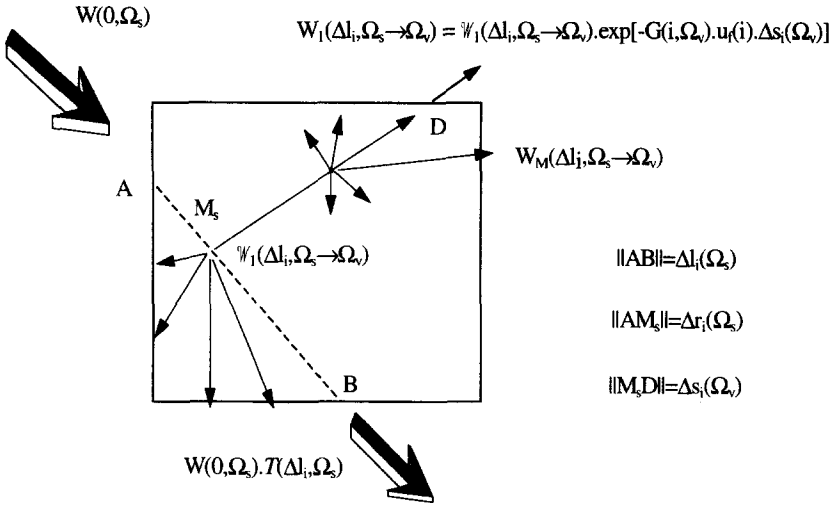

Figure 4. Within cell single and multiple scattering mechanisms.

the leaf scattering phase function $f(j,\Omega_f,\Omega_s\rightarrow\Omega_v)$ is the sum of a lambertian component $f_d(j,\Omega_f,\Omega_s\rightarrow\Omega_v)$ and a specular component $f_s(j,\Omega_f,\Omega_s\rightarrow\Omega_v)$. Examples of $f_d(j,\Omega_f,\Omega_s\rightarrow\Omega_v)$ and $f_s(j,\Omega_f,\Omega_s\rightarrow\Omega_v)$ functions are shown below. Then, the transfer function is the sum of two matrices associated with lambertian and specular components. The lambertian component, also called diffuse foliar component, is usually assumed to be due to radiation that penetrates the leaf to be absorbed by leaf metabolic constituents and to be multiply scattered at the leaf dielectric interfaces. This is randomly polarized and carries information about the leaf interior. On the other hand, the specular component is usually associated with radiation that does not penetrate the leaf and that is reflected by leaf surface; it does not contain information about the leaf mesophyll. Specularly reflected radiation is often assumed to be linearly polarized (Egan, 1985). It may represent an important proportion of total reflection; for example, 30%, 17%, and 2% of the total light reflected in the green (550 nm), red (630 nm), and near-infrared (790 nm) spectral regions, respectively, by a soybean canopy in the incidence plane at 30° view zenith angle with a −30° sun zenith angle (Rondeau and Herman, 1991).

Source vectors associated with leaf lambertian scattering, that is, photons having undergone at least one leaf volume scattering are noted $W_{df}(\Omega)$. Conversely, source vectors not associated with any leaf volume scattering are noted $W_{nf}(\Omega)$. Polarized source vectors are noted $W_p(\Omega)$. Thus, source vectors are three dimension vectors:

$$[W(\Omega),W_{nf}(\Omega),W_p(\Omega)] \qquad \text{with } W(\Omega)=W_{df}(\Omega)+W_{nf}(\Omega).$$

Proportions of leaf scattered radiation that arise from volume, surface, and polarization mechanisms are noted $df(\Omega)$, $nf(\Omega)$, and $p(\Omega)$, respectively, Thus, we have

$$W_{df}(\Omega)=df(\Omega)\cdot W(\Omega), \qquad W_{nf}(\Omega)=nf(\Omega)\cdot W(\Omega),$$
$$W_p(\Omega)=p(\Omega)\cdot W(\Omega), \qquad df(\Omega)+nf(\Omega)=1.$$

Thus, an unpolarized sun radiation incident on the scene is noted $[W(\Omega),W(\Omega),0]$.

Leaf Specular Reflection

According to Vanderbilt et al. (1991), leaf specular phase functions $f_s(j,\Omega_f,\Omega_s\rightarrow\Omega_v)$ are assumed to depend on three parameters: the angle Ψ_{fs} between the incident radiation (Ω_s) and the leaf normal (Ω_f), the surface refraction index n_j (≈ 1.5), and a parameter $K_j(\kappa,\Psi_{fs})$, between 0 and 1, that characterizes the smoothness of leaf cuticle:

$$f_s(j,\Omega_f,\Omega_s\rightarrow\Omega_v)=K_j(\kappa,\Psi_{fs})\cdot R_s^2(n_j,\Psi_{fs})\cdot\delta(\Omega_v,\Omega_v^*),$$

where $\delta(\Omega_v,\Delta_v^*)$ is a Dirac function; that is, $\delta(\Omega_v,\Omega_v^*)=0$ if Ω_v differs from the specular direction Ω_v^*. This is a function of incident direction (Ω_s) and leaf normal (Ω_f).

$R_s^2(n_j,\Psi_{fs})$ is the Fresnel reflectance averaged over the polarization states:

$$R_s^2(n_j,\Psi_{fs})=\frac{1}{2}\cdot\left[\frac{\sin^2(\Psi_{fs}-\theta)}{\sin^2(\Psi_{fs}+\theta)}+\frac{\tan^2(\Psi_{fs}-\theta)}{\tan^2(\Psi_{fs}+\theta)}\right],$$
$$\sin\theta=\frac{\sin\Psi_{fs}}{n_j}$$

The polarized component is

$$R_p^2(n_j,\Psi_{fs})=\frac{1}{2}\cdot\left[\frac{\sin^2(\Psi_{fs}-\theta)}{\sin^2(\Psi_{fs}+\theta)}-\frac{\tan^2(\Psi_{fs}-\theta)}{\tan^2(\Psi_{fs}+\theta)}\right].$$

Hereafter, polarization mechanisms are simulated in a very simple way: The polarization of incident radiation is not taken into account, and single scattering mechanisms are assumed to be the only mechanisms that give rise to polarization.

The specular flux $\mathscr{W}_s(\Delta l_i,\Omega_s\rightarrow\Omega_v)$ and the polarized flux $\mathscr{W}_p(\Delta l_i,\Omega_s\rightarrow\Omega_v)$ scattered along the direction (Ω_v), due to an intercepted flux $W_{int}(\Delta l_i,\Omega_s)$ are

$$\mathscr{W}_s(\Delta l_i,\Omega_s\rightarrow\Omega_v)=T_s(j,\Omega_s,\Omega_v)\cdot W_{int}(\Delta l_i,\Omega_s)$$

and

$$\mathscr{W}_p(\Delta l_i,\Omega_s\rightarrow\Omega_v)=T_p(j,\Omega_s,\Omega_v)\cdot W_{int}(\Delta l_i,\Omega_s),$$

with

$$T_s(j,\Omega_s,\Omega_v) \approx \frac{|\Omega_s \cdot \Omega_f^*| \cdot \frac{g_f(j,\Omega_f^*)}{2\pi} \cdot K_j(\kappa,\Psi_{fs}) \cdot R_s^2(n_j,\Psi_{fs})}{G(j,\Omega_s)} \cdot \Delta\Omega_f^*,$$

$$T_p(j,\Omega_s,\Omega_v) \approx \frac{|\Omega_s \cdot \Omega_f^*| \cdot \frac{g_f(j,\Omega_f^*)}{2\pi} \cdot K_j(\kappa,\Psi_{fs}) \cdot R_p^2(n_j,\Psi_{fs})}{G(j,\Omega_s)} \cdot \Delta\Omega_f^*.$$

The term $\Delta\Omega_f^*$ represents the solid angle that comprises all leaf normal directions that satisfy the conditions of specularity for the reflection $(\Omega_s,\Delta\Omega_s) \rightarrow (\Omega_v,\Delta\Omega_v)$:

$$\Omega_s \cdot \Omega_f = -\Omega_v \cdot \Omega_f \quad \text{and}$$

$$\begin{cases} \pi - a\cos(\Omega_s \cdot \Omega_v) = 2 \cdot a\cos(\Omega_v \cdot \Omega_f) & \text{if } \Omega_s \cdot \Omega_f < 0, \\ \pi - a\cos(\Omega_s \cdot \Omega_v) = -2 \cdot a\cos(\Omega_v \cdot \Omega_f) & \text{if } \Omega_s \cdot \Omega_f > 0. \end{cases}$$

According to Reyna and Badhwar (1985), the leaf normal direction $\Omega_f^* = (\theta_f^*, \varphi_f^*)$ that induces the specular reflection $(\Omega_s \rightarrow \Omega_v)$ is defined by

$$\cos\theta_f^* = \frac{|\cos\theta_s - \cos\theta_v|}{\sqrt{2(1-\Omega_s \cdot \Omega_v)}} \quad \text{and}$$

$$\tan\varphi_f^* = \frac{\sqrt{1-\cos^2\theta_s} \cdot \sin\varphi_s - \sqrt{1-\cos^2\theta_v} \cdot \sin\varphi_v}{\sqrt{1-\cos^2\theta_s} \cdot \cos\varphi_s - \sqrt{1-\cos^2\theta_v} \cdot \cos\varphi_v}.$$

Moreover, the angular cone of leaf normals that leads to the specular reflection is

$$\Delta\Omega_f^* = \frac{\left(\sqrt{\Delta\Omega_s} + \sqrt{\Delta\Omega_v}\right)^2}{4 \cdot |\Omega_s \cdot \Omega_f|} \quad \text{(Vanderbilt et al., 1991).}$$

For first-order scattering mechanisms associated with direct sun radiation, incident radiation is assumed to be monodirectional (i.e., $\Delta\Omega_s \approx 0$). So, $\Delta\Omega_f^* \approx \Delta\Omega_v / (4 \cdot |\Omega_s \cdot \Omega_f^*|)$. Then,

$$\mathscr{W}_s(\Delta l_i,\Omega_s \rightarrow \Omega_v) = \frac{W_{\text{int}}(\Delta l_i \cdot \Omega_s)}{G(j,\Omega_s)} \cdot \frac{g_f(j,\Omega_f^*)}{8\pi} \cdot K_j(\kappa,\Psi_{fs}^*) \cdot R_s^2(n_j,\Psi_{fs}^*) \cdot \Delta\Omega_v,$$

$$\mathscr{W}_p(\Delta l_i,\Omega_s \rightarrow \Omega_v) = \frac{W_{\text{int}}(\Delta l_i \cdot \Omega_s)}{G(j,\Omega_s)} \cdot \frac{g_f(j,\Omega_f^*)}{8\pi} \cdot K_j(\kappa,\Psi_{fs}^*) \cdot R_p^2(n_j,\Psi_{fs}^*) \cdot \Delta\Omega_v.$$

Leaf Lambertian Scattering

The lambertian behavior of leaf elements is modeled with the leaf hemispherical reflectance $\rho_{d,\text{leaf}}$ and transmittance $\tau_{d,\text{leaf}}$ coefficients:

$$f_d(j,\Omega_s \rightarrow \Omega_v,\Omega_f) = \begin{cases} \frac{1}{\pi} \cdot \rho_{d,\text{leaf}}(j,\Psi_{fs}) \cdot |\Omega_f \cdot \Omega_v|, & (\Omega_s \cdot \Omega_f) \cdot (\Omega_f \cdot \Omega_v) < 0, \\ \frac{1}{\pi} \cdot \tau_{d,\text{leaf}}(j,\Psi_{fs}) \cdot |\Omega_f,\Omega_v|, & (\Omega_s \cdot \Omega_f) \cdot (\Omega_f \cdot \Omega_v) < 0. \end{cases}$$

Use of this leaf scattering function in the general expression of the cell transfer function leads to the leaf cell diffuse transfer function $[T_d(j,\Omega_s,\Omega_v)]$.

Within Cell Single Scattering

Total within cell single scattering in the 4π space, due to an incident flux $W(0,\Omega_s)$, is

$$\mathscr{W}_1(\Delta l_i,\Omega_s) = \int_{4\pi} \mathscr{A}(\Delta l_i,\Omega_s \rightarrow \Omega_v) \cdot d\Omega_v = \sum_{v=1}^{N} [\mathscr{W}_{d1}(\Delta l_i,\Omega_s \rightarrow \Omega_v) + \mathscr{W}_{s1}(\Delta l_i,\Omega_s \rightarrow \Omega_v)], \quad v \in [1\ N],$$

where $\mathscr{W}_{d1}(\Delta l_i,\Omega_s \rightarrow \Omega_v)$ and $\mathscr{W}_{s1}(\Delta l_i,\Omega_s \rightarrow \Omega_v)$ are the single scattered source vectors associated with the scattering transfer functions $T_d(j,\Omega_s,\Omega_v)$ and $T_s(j,\Omega_s,\Omega_v)$.

In fact, the flux $\mathscr{W}_1(\Delta l_i,\Omega_s,\rightarrow \Omega_v)$ undergoes further inception and scattering before escaping the cell. Transmission along (Ω_v) within the cell is computed with the assumption that the scattered flux $\mathscr{W}(\Delta l_i,\Omega_s \rightarrow \Omega_v)$ originates from a unique point, called middle point (M_s), within the cell i, and not from the cell center. Simulation of scattering mechanisms from (M_s) instead of the cell center leads to more accurate results, especially for cells with large u_f values and for oblique propagation directions. In a second step, the geometrical propagation of scattered radiation that has already gone out of the cell is simulated from the cell center. The point (M_s) is defined as the point along the path $(\Delta l_i,\Omega_s)$ such that 50% of the total intercepted radiation $W_{\text{int}}(\Delta l_i,\Omega_s)$ is intercepted before this point. The pathlength between (M_s) and the entrance point of cell i is called Δr_i. We have

$$\int_{4\pi} \mathscr{A}(\Delta r_i,\Omega_s \rightarrow \Omega_v) \cdot d\Omega_v = \frac{1}{2} \cdot \int_{4\pi} \mathscr{A}(\Delta l_i,\Omega_s \rightarrow \Omega_v) \cdot d\Omega_v$$

$$\Rightarrow \quad \Delta r_i = \frac{\ln 2 - \ln[1 + \exp(-u_f(i) \cdot G(j,\Omega_s) \cdot \Delta l_i)]}{u_f(i) \cdot G(j,\Omega_s)}. \tag{8}$$

The scattered radiation $W_1(\Delta l_i,\Omega_s \rightarrow \Omega_v)$ that escapes cell i along (Ω_v) corresponds to the attenuation of $\mathscr{W}_1(\Delta l_i,\Omega_s \rightarrow \Omega_v)$ within cell i after a propagation length $\Delta s_i(\Omega_v)$ from the middle point (M_s). It is a single-scattering radiation:

$$W_1(\Delta l_i,\Omega_s \rightarrow \Omega_v) = \mathscr{W}_1(\Delta l_i,\Omega_s \rightarrow \Omega_v) \cdot \exp[-G(j,\Omega_v) \cdot u_f(i) \cdot \Delta s_i(\Omega_v)].$$

This term is the sum of a diffuse and a specular component:

$$W_{d1}(\Delta l_i,\Omega_s \rightarrow \Omega_v) = \mathscr{W}_{d1}(\Delta l_i,\Omega_s \rightarrow \Omega_v) \cdot \exp[-G(j,\Omega_v) \cdot u_f(i) \cdot \Delta s_i(\Omega_v)],$$

$$W_{s1}(\Delta l_i,\Omega_s \rightarrow \Omega_v) = \mathscr{W}_{s1}(\Delta l_i,\Omega_s \rightarrow \Omega_v) \cdot \exp[-G(j,\Omega_v) \cdot u_f(i) \cdot \Delta s_i(\Omega_v)].$$

Thus, with a radiation $[W_{\text{in}}(0,\Omega_s), W_{nf,\text{in}}(\Omega_s), W_{p,\text{in}}(\Omega_s)]$ incident on a cell i of type j, the single-scattering source vector that escapes cell i along direction (Ω_v) is

$$[W_1(\Delta l_i,\Omega_s \rightarrow \Omega_v),\ W_{nf,1}(\Delta l_i,\Omega_s \rightarrow \Omega_v),\ W_{p,1}(\Delta l_i,\Omega_s \rightarrow \Omega_v],$$

where

$$W_1(\Delta l_i,\Omega_s\rightarrow\Omega_v) = T(\Delta s_i,\Omega_v)\cdot T(j,\Omega_s,\Omega_v) \cdot(1 - T(\Delta l_i,\Omega_s))\cdot W_{in}(0,\Omega_s), \quad (9a)$$

$$W_{nf,1}(\Delta l_i,\Omega_s\rightarrow\Omega_v) = T(\Delta s_i,\Omega_v)\cdot T_s(j,\Omega_s,\Omega_v) \cdot(1 - T(\Delta l_i,\Omega_s))\cdot W_{nf,in}(0,\Omega_s),$$

$$W_{nf,1}(\Delta l_i,\Omega_s\rightarrow\Omega_v) = nf_1(\Omega_s,\Omega_v)\cdot W_1(\Delta l_i,\Omega_s\rightarrow\Omega_v), \quad (9b)$$

$$W_{p,1}(\Delta l_i,\Omega_s\rightarrow\Omega_v) = T(\Delta s_i,\Omega_v)\cdot T_p(j,\Omega_s,\Omega_v) \cdot(1 - T(\Delta l_i\Omega_s))\cdot W_{in}(0,\Omega_s),$$

$$W_{p,1}(\Delta l_i,\Omega_s\rightarrow\Omega_v) = p_1(j,\Omega_s,\Omega_v)\cdot W_1(\Delta l_i,\Omega_s\rightarrow\Omega_v), \quad (9c)$$

with

$$nf_1(\Omega_s,\Omega_v) = \frac{W_{nf,1}(\Delta l_i,\Omega_s\rightarrow\Omega_v)}{W_1(\Delta l_i,\Omega_s\rightarrow\Omega_v)} = s_1(j,\Omega_s,\Omega_v)\cdot nf_{in}(\Omega_s),$$

$$s_1(j,\Omega_s,\Omega_v) = \frac{T_s(j,\Omega_s,\Omega_v)}{T(j,\Omega_s,\Omega_v)},$$

$$p_1(j,\Omega_s,\Omega_v) = \frac{W_{p,1}(\Delta l_i,\Omega_s\rightarrow\Omega_v)}{W_1(\Delta l_i,\Omega_s\rightarrow\Omega_v)} = \frac{T_p(j,\Omega_s,\Omega_v)}{T(j,\Omega_s,\Omega_v)}.$$

Within Cell Multiple Scattering

Simulation of multiple scattering mechanisms is described in the Appendix. It is conducted without taking into account polarization mechanisms. It relies on the computation of the energy $\mathscr{W}_{1,int}(\Delta l_i,\Omega_s\rightarrow\Omega_v)$ intercepted along the path $\Delta s_i(\Omega_v)$. Because multiple scattering of this energy cannot be modeled exactly, we assume that radiation that has undergone more than one scattering within a cell is nearly isotropic. This assumption allows one to define the mean single scattering diffuse ω_{dj} and specular ω_{sj} albedos, for cells of type j, and the mean transmission coefficient $\langle T_i\rangle$ within any cell i. This leads to the computation of the multiple-scattering source vectors that escape any cell i; that is, total multiple-scattering source vectors $W_M(\Delta l_i,\Omega_s)$ and $W_M(\Delta l_i,\ \Omega_s\rightarrow\ \Omega_v)$, specular source vectors $W_{sM}(\Delta l_i,\Omega_s)$ and $W_{sM}(\Delta l_i,\Omega_s\rightarrow\Omega_v)$, and source vectors $W_{nf,M}(\Delta l_i,\Omega_s\rightarrow\ \Omega_v)$ not associated with at least one leaf volume scattering.

Thus, the multiple-scattering source vector that escapes cell i along (Ω_v) is

$$[W_M(\Delta l_i,\Omega_s\rightarrow\Omega_v), W_{nf,M}(\Delta l_i,\Omega_s\rightarrow\Omega_v), 0].$$

Finally, the total scattered source vector, that is, single and multiple scattering radiation, along direction (Ω_v) is

$$[W_1(\Delta l_i,\Omega_s\rightarrow\Omega_v) + W_M(\Delta l_i,\Omega_s\rightarrow\Omega_v), W_{nf,1}(\Omega_v) + W_{nf,M}(\Omega_v), W_{p,1}(\Omega_v)]. \quad (10)$$

The absorbed source vector associated with the incident source vector $W(0,\Omega_s)$ is

$$W_a(\Delta l_i,\Omega_s) = [W_{int}(\Delta l_i,\Omega_s) - \mathscr{W}_1(\Delta l_i,\Omega_s)] + \sum_{v=1}^{N}\{\mathscr{W}_{1,int}(\Delta l_i,\Omega_s\rightarrow\Omega_v) - W_M(\Delta l_i,\Omega_s\rightarrow\Omega_v)\}.$$

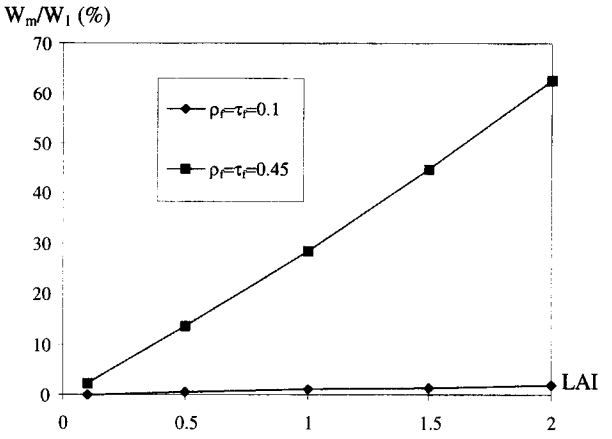

Figure 5. Ratio $W_M(\Delta l_i,\Omega_s\rightarrow\Omega_v)$ / $W_1(\Delta l_i,\Omega_s\rightarrow\Omega_v)$ of a leaf cell as a function of cell LAI. Two cases are considered: $\omega_d = 0.9$ and $\omega_d = 0.2$. The LAD is spherical and leaf specular reflectance is neglected.

Figure 5 shows the relative importance of single-scattering $W_1(\Delta l_i,\Omega_s\rightarrow\Omega_v)$ and multiple-scattering $W_M(\Delta l_i,\Omega_s\rightarrow\Omega_v)$ source vectors, in the case of a foliar cell j with a spherical LAD, as a function of the cell LAI. Leaf specular reflectance is neglected. Two cases are considered: $\omega_j = 0.9$, $\rho_d = \tau_d = 0.45$, and $\omega_j = 0.2$, $\rho_d = \tau_d = 0.1$. It appears that $W_M(\Delta l_i,\Omega_s\rightarrow\Omega_v)$ is all the more important compared to $W_1(\Delta l_i,\Omega_s\rightarrow\Omega_v)$ than the LAI is large and than the leaf single-scattering albedo is large. For example, with $\omega_j = 0.9$ and LAI = 2, $W_M(\Delta l_i,\Omega_s\rightarrow\Omega_v)$ is equal to 63% of $W_1(\Delta l_i,\Omega_s\rightarrow\Omega_v)$. This clearly stresses that the multiple-scattering component must not be neglected.

The above-mentioned single and multiple scattering mechanisms occur for each iteration of the DART model. Some simplifications are introduced for multiple scattering, to reduce computation times; they are shown in the following section.

Hot Spot Effect

The finite size of scatterers within the canopy is responsible of the peak in reflected radiation in the retroillumination direction. This is the well known hot spot effect. According to many authors (Qin and Xiang, 1994), this may be a diagnostic tool for canopy structure because its magnitude depends on the size, shape, density, orientation, and spatial distribution of foliage elements. For example, in the case of tree canopies its width is often assumed to be governed by the elliptical shape of crowns (Barker Schaaf and Stralher, 1994). In a homogeneous medium, attenuation mechanisms that occur along the scattering direction (Ω_v) are more or less correlated with those occurring in the incident downward direction (Ω_s), depending on the closeness of directions (Ω_s) and (Ω_v); the correlation value depends on the scattering angle, and on the size s_f of the scatterers vs. their depth in the foliar medium. Here, the approach of Kuusk (1985) is adapted in order to take into account the fact

that cells are not infinite horizontal media. It results that the extinction coefficient along direction (Ω_v) of single-scattering source vector $[W_1(\Delta l_i,\Omega_s\rightarrow\Omega_v)]$ at a distance $\delta s_i(\Omega_v)$ from the origin point in cell i where reflection took place is not $u_f(i)\cdot G(i,\Omega_v)$, but

$$a_a(\Omega_s,\Omega_v,\delta S_i)=$$

$$u_f(i)\cdot G(i,\Omega_v)\cdot\left[1-\sqrt{\frac{G(\Omega_s)\cdot\mu_v}{G(\Omega_v)\cdot|\mu_s|}}\cdot\exp\left[-\frac{\Delta(\Omega_s,\Omega_v)}{Sf}\cdot\delta s_i(\Omega_v)\cdot\mu_v\right]\right]$$

where

$$\Delta(\Omega_s,\Omega_v)=\sqrt{\frac{1}{\mu_v^2}+\frac{1}{\mu_s^2}-\frac{2\cdot\cos\ a}{|\mu_s\cdot\mu_v|}}\qquad\text{and}\qquad\cos\ a=\Omega_s\cdot\Omega_v.$$

The attenuation of $W_l(\Delta l_{ij},\Omega_s\rightarrow\Omega_v)$ along the path $\Delta s_i(\Omega_v)$ is $\exp\left[-\int_{\Delta S_i(\Omega_v)}a_a(\Omega_s,\Omega_v,r)\cdot dr\right]$.

It must be noted that the hot spot effect is not applied to multiple-scattering source vectors, that is, source vectors $W_M(\Delta l_i,\Omega_s\rightarrow\Omega_v)$ in all iterations and source vectors $W_1(\Delta l_i,\Omega_s\rightarrow\Omega_v)$ in iterations larger than 1.

Iterative Processes with Single and Multiple Scattering

As mentioned above, the DART simulation procedure relies on an iterative method. Two different approaches are adopted for simulating cell interaction mechanisms in the first iteration, that is, mostly single scattering, and in the following iterations.

First Iteration: $k=1$, $nf_{in}(\Omega_s)=1$, and $\Omega_s=\Omega_{sun}$

The only incident source vector, that is, attenuated direct sun radiation, is a nonfoliar flux ($nf_{in}(\Omega_s)=1$) assumed to be nonpolarized ($p_{in}(\Omega_s)=0$). This sun source vector $[W_{in}(0,\Omega_s),W_{in}(0,\Omega_s),0]$ incident on cell i, along the path $(\Delta l_i,\Omega_s)$, gives rise to a scattered source vector that escapes cell i along direction (Ω_v):

$$[W_{scat}(\Delta l_i,\Omega_s\rightarrow\Omega_v),W_{nf}(\Delta l_i,\Omega_s\rightarrow\Omega_v),W_p(\Delta l_i,\Omega_s\rightarrow\Omega_v)]$$

with

$$W_{scat}(\Delta l_i,\Omega_s\rightarrow\Omega_v)=W_1(\Delta l_i,\Omega_s\rightarrow\Omega_v)+W_M(\Delta l_i,\Omega_s\rightarrow\Omega_v),$$

$$W_{nf}(\Delta l_i,\Omega_s\rightarrow\Omega_v)=s_1(j,\Omega_s,\Omega_v\cdot W_1(\Delta l_i,\Omega_s\rightarrow\Omega_v)+\frac{\omega_{sj}}{\omega_j}\cdot\frac{T(\Delta s_i,\Omega_v)}{\langle T_i\rangle}\cdot s_M(j,\Omega_v)\cdot W_{sM}(\Delta l_i,\Omega_s),$$

$$W_p(\Delta l_i,\Omega_s\rightarrow\Omega_v)=p_1(j,\Omega_s,\Omega_v)\cdot W_1(\Delta l_i,\Omega_s\rightarrow\Omega_v).$$

So, we have

$$nf(\Delta l_i,\Omega_s,\Omega_v)=\frac{s_l(j,\Omega_s,\Omega_v)\cdot W_1(\Delta l_i,\Omega_s\rightarrow\Omega_v)+\frac{T(\Delta s_i,\Omega_v)}{\langle T_i\rangle}\cdot s_M(j,\Omega_v)\cdot\frac{\omega_{sj}}{\omega_j}\cdot W_{sM}(\Delta l_i,\Omega_s)}{W_{scat}(\Delta l_i,\Omega_s\rightarrow\Omega_v)},$$

$$p(\Delta l_i,\Omega_s,\Omega_v)=\frac{p_l(j,\Omega_s\Omega_v)\cdot W_1(\Delta l_i,\Omega_s\rightarrow\Omega_v)}{W_{scat}(\Delta l_i,\Omega_s\rightarrow\Omega_v)}.$$

In fact, each cell can be irradiated by different source vectors that propagate along the same direction (Ω_s). We call $\mathscr{O}$ this total number of incident source vectors. The latter are noted $W_{in}(o,\Omega_s)$, with $o\in[1\ \ \mathscr{O}]$. Consequently, total scattered radiation that escapes cell i along direction (Ω_v) is

$$\left[\sum_{o=1}^{\mathscr{O}}W_{scat}(\Delta l_i(o),\Omega_s\rightarrow\Omega_v,W_{nf}(\Omega_v),W_p(\Omega_v)\right]\qquad\text{with } o\in[1\ \ \mathscr{O}],$$

with

$$W_{nf}(\Omega_v)=\sum_{o=1}^{\mathscr{O}}W_{nf}(\Delta l_i(o)\Omega_s\rightarrow\Omega_v)=\sum_{o=1}^{\mathscr{O}}nf(\Delta l_i(o),\Omega_s,\Omega_v)\cdot W_{scat}(\Delta l_i(o),\Omega_s\rightarrow\Omega_v),$$

$$W_p(\Omega_v)=\sum_{o=1}^{\mathscr{O}}W_p(\Delta l_i(o),\Omega_s\rightarrow\Omega_v)=\sum_{o=1}^{\mathscr{O}}p(\Delta l_i(o),\Omega_s,\Omega_v)\cdot W_{scat}(\Delta l_i(o)\Omega_s\rightarrow\Omega_v).$$

For each interaction (i.e., $\mathscr{O}$ interactions) the intercepted radiation $W_{int}(\Delta l_i,(o),\Omega_s)$ and the coordinates of the associated middle point (M_s) are stored. Indeed, these only quantities allow one to compute $W_1(\Delta l_i,\Omega_s\rightarrow\Omega_v)$ and $W_M(\Delta l_i,\Omega_s\rightarrow\Omega_v)$. The scalar summation of $W_p(\Delta l_i(o),\Omega_s\rightarrow\Omega_v)$ vector sources is only possible because all scattered source vectors are assumed to have identical polarization directions. In the following iteration, cells that have intercepted source vectors in the first iteration become secondary sources.

Further Iterations: $k>1$ and $\Omega_s\in4\pi$

Incident source vectors $[W_{in}(0,\Omega_n),W_{nf,in}(\Omega_n),W_{p,in}(\Omega_n)]$ stand for already scattered radiation and atmospheric radiation. In a first approximation, considering that incident radiation tends to be isotropic, the polarized scattered component is simply assumed to be nil. Thus, with a source vector incident on cell i along the path $(\Delta l_i,\Omega_n)$, the source vector that escapes this cell along direction Ω_v) is

$$[W_{scat}(\Delta l_i,\Omega_n\rightarrow\Omega_v),W_{nf}(\Delta l_i\Omega_n\rightarrow\Omega_v),0],$$

with

$$W_{scat}(\Delta l_i,\Omega_n\rightarrow\Omega_v)=W_1(\Delta l_i,\Omega_n\rightarrow\Omega_v)+W_M(\Delta l_i\Omega_n\rightarrow\Omega_v),$$

$$W_{nf}(\Delta l_i,\Omega_n\rightarrow\Omega_v)=nf_{in}(\Omega_n)\cdot\left[s_1(j,\Omega_n,\Omega_v)\cdot W_1(\Delta l_i,\Omega_n\rightarrow\Omega_v)+\frac{T(\Delta s_i,\Omega_v)}{\langle T_i\rangle}\cdot s_M(j,\Omega_v)\cdot\frac{\omega_{sj}}{\omega_j}W_{sM}(\Delta l_i,\Omega_s)\right].$$

In fact, each cell is irradiated by a number $\mathscr{O}$ of source vectors $\mathscr{W}_{in}(\Omega_{ni(o)})$ that propagate along different incident directions $\Omega_{n(o)}$ in the 4π space, with $o\in[1\ \mathscr{O}]$ and $n\varepsilon\ [1\ \mathscr{N}]$. Consequently, total scattered radiation $[W_{scat}(\mathscr{O},\Omega_v)]$ that escapes cell i along direction (Ω_v) is

$$\left[\sum_{o=1}^{\mathcal{O}} W_{\text{scat}}(\Delta l_i(o),\Omega_{n(o)}\rightarrow\Omega_v), \sum_{o=1}^{\mathcal{O}} W_{nf}(\Delta l_i(o),\Omega_{n(o)}\rightarrow\Omega_v), 0\right].$$

Use of the approach of iteration 1 would lead to store all middle points $M_s(o)$, the intercepted radiation W_{int} $(\Delta l_i,\Omega_{n(o)})$, and the associated incident directions $(\Omega_{n(o)})$, with $o\in[1\ \ \mathcal{O}]$. This would demand a huge computer memory capacity with large scenes. Thus, another approach is adopted. When an incident radiation $[W(0,\Omega_n)]$, with $n\in[1\ \ \mathcal{N}]$, is intercepted, resulting scattered specific intensities $I(\Delta l_i,\Omega_n\rightarrow\Omega_v)$ and $I_{nf}(\Delta l_i,\Omega_n\rightarrow\Omega_v)$, associated with source vectors $W(\Delta l_i,\Omega_n\rightarrow\Omega_v)$ and $W_{nf}(\Delta l_i,\Omega_n\rightarrow\Omega_v)$, are computed for all $N(\Omega_v)$ directions, and their distribution is represented by a spherical expansion:

$$I(\Delta l_i,\Omega_n\rightarrow\Omega_v)=\sum_{l=0}^{l=L}\sum_{m=-l}^{m=l} C_{lm}(i,k)\cdot Y_{lm}(\theta,\varphi),$$

where $Y_{lm}(\theta,\varphi)$ are the normalized spherical harmonics and C_{lm} the associated coefficients. L is an integer number that indicates the order of the expansion. It can be selected by the operator. In real form the normalized spherical harmonics are defined by

$$Y_{lm}(\theta,\varphi)=\begin{cases} N_{lm}\cdot P_{lm}(\cos\ \theta)\cdot\cos(m\varphi) & \text{if } m>0,\\ N_{lo}\cdot P_{lo}(\cos\ \theta)/\sqrt{2} & \text{if } m=0,\\ N_{lm}\cdot P_{lm}(\cos\ \theta)\cdot\sin(|m|\varphi) & \text{if } m<0,\end{cases}$$

where the $P_{lm}(x)$ factors are the associated Legendre polynomials and the normalizing constants N_{lm} are given by

$$N_{lm}=\sqrt{\frac{2l+1}{2\pi}\cdot\frac{(1-|m|)!}{(1+|m|)!}}.$$

The $C_{lm}(i,k)$ coefficients related to the kth scattering order in cell i are derived from

$$C_{lm}(i,k,\Omega_s)=\int_0^{2\pi}\int_0^{\pi} I(\Delta l_i,\Omega_s\rightarrow\Omega)\cdot Y_{lm}(\theta,\varphi)\cdot\sin\ \theta\cdot d\varphi\cdot d\theta$$
$$=\sum_{v=1}^{N} W_{\text{scat}}(\Omega_s\rightarrow\Omega_v)\cdot Y_{lm}(\Omega_v).$$

The coefficients $C_{lm}(i,k,\Omega_s)$ are actually computed during the $(k-1)$th iteration order, both for the total $W_{\text{scat}}(\Omega_v)$ and the nonfoliar $W_{nf}(\Omega_v)$ radiation components. After each interaction with cell i, the new C_{lm} coefficients are added to the C_{lm} coefficients associated with radiation previously scattered in that cell:

$$C_{lm}(i,k)=\sum_{o=1}^{\mathcal{O}} C_{lm}(i,k,\Omega_s),\quad \text{where } \mathcal{O} \text{ is the total number of radiation incident on cell } i.$$

The scattered source vector $[W_{\text{scat}}(i,\Omega_v),\ W_{nf,\text{scat}}(i,\Omega_v),\ 0]$ that exits cell i is computed in the kth iteration:

$$W_{\text{scat}}(i,\Omega_v)=\sum_{l=0}^{l=L}\sum_{m=-l}^{m=l} C_{lm}(i,k)\cdot Y_{lm}(\Omega_v)\cdot\Delta\Omega_v,$$

$$W_{nf,\text{scat}}(i,\Omega_v)=\sum_{l=0}^{l=L}\sum_{m=-l}^{m=l} C_{lm,nf}(i,k)\cdot Y_{lm}(\Omega_v)\cdot\Delta\Omega_v.$$

The spherical harmonics formulation may not be well adapted if the transfer matrix is very anisotropic. Such an anisotropy occurs with opaque media such as soils. For example, an horizontal opaque surface displays a discontinuity of the scattered flux for directions within the plane of the interface. Moreover, it may comprise a strong specular component, for example, due to direct sun illumination. In the presence of such surfaces the following approach must be adopted: Before computing the C_{lm} coefficients, the transfer matrix is extended to the forward hemisphere. Thus, in the special case of an horizontal surface, we use the relation

$$I(i,\pi-\theta,\varphi)=I(i,\theta,\varphi).$$

This approach is interesting because it smoothes the integrated term $I(i,\theta,\varphi)$, which results in a more accurate approximation with a fixed number of C_{lm} coefficients. This extension is especially designed for soil and water cells.

The spherical harmonics expansion is well adapted to approximate relatively smooth functions defined on the sphere, with a finite number of terms. This number is much less important than the total number N of discrete directions. A diffuse smoothly varying distribution of specific intensity will typically require fewer coefficients than a very directional one. Moreover, the spherical harmonics expansion is well adapted to the incremental computation of scattered radiation resulting from successive impinging interaction mechanisms, for each cell. After a scattering event occurs in cell i, we have the following sequence of operations: computation of the angular distribution of the scattered source vector $W(i,\Omega_v)$ and $W_{nf}(i,\Omega_v)$, computation of the associated C_{lm} and $C_{lm,nf}$ coefficients, and adding these coefficients to the already accumulated $C_{lm}(i)$ and $C_{lm,nf}(i)$ coefficients.

The spherical harmonics expansion is not used during iteration 1. Indeed, the simple knowledge of the intercepted radiation and of the associated middle point, combined with the fact that sun direction is known, is less computer memory demanding than the spherical harmonics-based approach. Moreover, and above all, it leads to more accurate results because scattered radiation that results from monodirectional incident radiation may be highly anisotropic, which is poorly represented by a spherical harmonics expansion with a limited number of terms.

Interaction Mechanisms of Nonleaf Cells

Interaction mechanisms associated with non leaf cells are briefly introduced below.

Soil Cells

Their optical properties are represented by scattering transfer matrices $T_{\text{soil}}(\Omega_s,\Omega_v)$ derived from measurements

or computations with whatever available soil bidirectional reflectance model. Associated polarization transfer matrices are noted $T_{p,soil}(\Omega_s,\Omega_v)$. Only surface interactions are simulated. The geometrical path of a soil scattered radiation within the scene is simulated from the center of the irradiated soil cell face. In order to take into account topography, soil cell interactions are handled separately for each cell face. So, during the direct sun illumination phase, the energy intercepted is stored for each individual face of soil cells. In the following iteration each face gives rise to secondary source vectors, with *a priori* defined scattering directions, for example, an upper horizontal face scatters upwards only. Similarly, during subsequent iterations, radiation interactions occur also on individual faces, and C_{lm} coefficients are computed and stored for each illuminated face of soil cells.

In a first approximation, polarization is simulated, independently of the polarization degree of the incident radiation. Naturally, any radiation scattered by a soil cell of type j has the same non foliar factor $nf_{in}(\Omega)$ as the incident radiation $[W_{in}(0,\Omega_s)]$. Thus, the resulting scattered source vector along direction (Ω_v) is

$$[W_{scat}(\Omega_v), W_{nf,scat}(\Omega_v), W_{p,scat}(\Omega_v)],$$

with

$$W_{scat}(\Omega_v) = T_{soil}(j,\Omega_s\Omega_v)\cdot W_{in}(0,\Omega_s),$$

$$W_{nf,scat}(\Omega_v) = nf_{in}(\Omega_s)\cdot W_{scat}(\Omega_v) \quad \text{and}$$

$$W_{p,scat}(\Omega_v) = T_{p,soil}(j,\Omega_s,\Omega_v)\cdot W_{in}(0,\Omega_s).$$

The expression of source vectors scattered by a soil cell depend on the iteration order:

Iteration $k=1$:

$$W_{scat}(\Omega_v) = \sum_{o=1}^{\mathcal{O}} T_{soil}(j,\Omega_s,\Omega_v)\cdot W_{in}(0,\Omega_s(o)) = T_{soil}(j,\Omega_s,\Omega_v)\cdot \sum_{o=1}^{\mathcal{O}} W_{in}(0,\Omega_s(o)),$$

$$W_{nf,scat}(\Omega_v) = \sum_{o=1}^{\mathcal{O}} W_{nf,scat}(\Omega_s(o)\rightarrow\Omega_v) = W_{scat}(\Omega_v),$$

$$W_{p,scat}(\Omega_v) = p_l(j,\Omega_s,\Omega_v)\cdot W_{scat}(\Omega_v) \quad \text{with}$$

$$p_l(j,\Omega_s,\Omega_v) = \frac{T_{p,soil}(j,\Omega_s,\Omega_v)}{T_{soil}(j,\Omega_s,\Omega_v)}.$$

Iteration $k>1$:

$$W_{scat}(\Omega_v) = \sum_{o=1}^{\mathcal{O}} T_{soil}(j,\Omega_{n(o)},\Omega_v)\cdot W_{in}(0,\Omega_{n(o)}),$$

$$W_{nf,scat}(\Omega_v) = \sum_{o=1}^{\mathcal{O}} nf_{in}(\Omega_{n(o)})\cdot W_{scat}(\Omega_{n(o)}\rightarrow\Omega_v),$$

$$W_{p,scat}(\Omega_v) = 0.$$

Trunk Cells

Trunk cells are undoubtedly of minor importance in many cases. Trunk cells are characterized by scattering $T_{trunk}(\Omega_n\rightarrow\Omega_v)$ and polarization $T_{p,trunk}(\Omega_n\rightarrow\Omega_v)$ transfer matrices. Polarization mechanisms are modeled without taking into account the polarization of the incident radiation $W_{in}(0,\Omega_s)$. For example, each trunk cell can be characterized by an hemispheric reflectance coefficient ρ_{trunk} and an extinction parameter η. The latter is independent of the incident radiation (Ω) and equal to the ratio of the vertical trunk surface by the surface of the associated vertical cell face. In fact, several trunk cells may be crossed when a source vector $W(\Omega_n)$ encounters a trunk. Let η_{max} be the maximum value of the η terms associated with the cells that are crossed. Then, the transmission coefficient of the incident source vector $W(\Omega_n)$ is

$$T(\Omega) = 1 - \eta_{max}.$$

Thus, $T(\Omega)\rightarrow 1$ if $\eta_{max}\rightarrow 0$ (i.e., empty cell) and $\eta_{max}\rightarrow 1$ if $T(\Omega)\rightarrow 0$ (i.e., 100% trunk cell).

So, in a first approximation the trunk scattering transfer matrix $T_{trunk}(\Omega_n\rightarrow\Omega_v)$ can be simply defined by

$$T_{trunk}(\Omega_n\rightarrow\Omega_v) = \frac{W_{scat}(\Omega_n\rightarrow\Omega_v)}{W_{in}(0,\Omega_n)} = \frac{\rho_{trunk}}{\pi}\cdot|\Omega_c\cdot\Omega_v|\cdot\eta_{max}\cdot\Delta\Omega_v,$$

where Ω_c is the direction normal to the irradiated cell faces.

Radiation interaction with trunk cells are processed on a face per face basis, in the same way as soil cells. The six faces can become secondary scatterers. In fact, source vectors are scattered only by cell faces that are directly irradiated by the incident radiation. Naturally, a source vector scattered by a trunk cell has the same non foliar component $nf(\Omega)$ as incident radiation. Thus, a number $\mathcal{O}$ of incident source vectors $[W_{in}(0,\Omega_{n(o)})]$ leads to

$$\left[\sum_{o=1}^{\mathcal{O}} W_{scat}(\Omega_{n(o)}\rightarrow\Omega_v), W_{nf,scat}(\Omega_v, W_{p,scat}(\Omega_v)\right].$$

Iteration $k=1$:

$$W_{nf,scat}(\Omega_s\rightarrow\Omega_v) = \sum_{o=1}^{\mathcal{O}} W_{scat}(\Omega_s(o)\rightarrow\Omega_v),$$

$$W_{p,scat}(\Omega_v) = \sum_{o=1}^{\mathcal{O}} p_l(j,\Omega_s,\Omega_v)\cdot W_{scat}(\Delta l_i(o),\Omega_s\rightarrow\Omega_v) = p_1(j,\Omega_s,\Omega_v)\cdot W_{scat}(\Omega_v).$$

Iteration $k>1$:

$$W_{nf,scat}(\Omega_v) = \sum_{o=1}^{\mathcal{O}} nf_{in}(\Omega_{n(o)})\cdot W_{scat}(\Omega_{n(o)}\rightarrow\Omega_v),$$

$$W_{p,scat}(\Omega_v) = 0.$$

Water Cells

Similarly to soil surfaces, water surfaces are modeled as a unique layer of water cells, and their upward reflectance characteristics are represented by scattering transfer functions $T_{water}(\Omega_s,\Omega_v)$ and polarized transfer functions

$T_{p,\text{water}}(\Omega_s,\Omega_v)$. These transfer functions are $N' \times N''$ transfer matrices, where N' and N'' are the number of downward and upward discrete directions, respectively ($N' + N'' = N$). The geometrical path within the scene of a water scattered radiation is simulated from the center of the irradiated water cell face. During the direct sun illumination phase, the energy intercepted by water cells is stored. These cells give rise to secondary source vectors in the following iteration.

Transfer matrices $T_{\text{water}}(\Omega_s,\Omega_v)$ and $T_{p,\text{water}}(\Omega_s,\Omega_v)$ may be derived from measurements or model simulations. An example of computation is shown below. Water may be assumed to give rise to a lambertian component, associated with volume reflection, and a specular component, associated with surface reflection. Naturally, any water cell scattered radiation has the same nonfoliar component $nf(\Omega)$ as the incident radiation.

1. Specular reflection: The specular source vector, and its associated polarized component are computed with Fresnel equations. The original polarization degree $p_{\text{in}}(\Omega_s)$ of the incident source vector is not taken into account; in fact, $p_{\text{in}}(\Omega_s)$ is assumed to be nil. Specular reflection occurs along a direction (Ω_v^*) such that $\theta_v^* = \pi - \theta_s$ and $\varphi_v = \varphi_s$. So, an incident source vector $W_{\text{in}}(\Omega_v)$ leads to a scattered source vector:

$$[W_{\text{spe}}(\Omega_s \rightarrow \Omega_v), nf_{\text{in}}(\Omega_s) \cdot W_{\text{spe}}(\Omega_s \rightarrow \Omega_v), p_{s,\text{scat}}(\Omega_v) \cdot W_{\text{spe}}(\Omega_s \rightarrow \Omega_v)],$$

where $W_{\text{spe}}(\Omega_s \rightarrow \Omega_v) = R_s^2(n,\theta_s) \cdot \delta(\Omega_v,\Omega_v^*) \cdot W_{\text{in}}(0,\Omega_s)$, n is the water refraction index, and $p_{s,\text{scat}}(\Omega_v) = R_p^2(n,\theta_s) / R_s^2(n,\theta_s)$.

2. Volume scattering: Volume scattering is assumed to be nonpolarized. In a first approximation, it can be simulated with a lambertian reflectance factor ρ_w. This input parameter is supposed to take into account water cells characteristics such as water depth, water turbidity, and the underlying soil surface, if necessary.

It results that source vectors that exit a water cell, illuminated by an incident source vector $[W_{\text{in}}(0,\Omega_s), W_{nf,\text{in}}(0,\Omega_s), W_{p,\text{in}}(0,\Omega_s)]$, are

$$[W_{\text{scat}}(\Omega_v), nf_{\text{in}}(\Omega_s) \cdot W_{\text{scat}}(\Omega_v), W_{p,\text{scat}}(\Omega_v)],$$

with

$$W_{\text{scat}}(\Omega_v) = \{(\rho_w / \pi) \cdot |\Omega_v \cdot \Omega_c| \cdot [1 - R_s^2(n,\theta_s)] \cdot \Delta\Omega_v + R_s^2(n,\theta_s) \cdot \delta(\Omega_v,\Omega_v^*)\} \cdot W_{\text{in}}(0,\Omega_s),$$

$$W_{p,\text{scat}}(\Omega_v) = R_p^2(n,\theta_s) \cdot W_{\text{in}}(0,\Omega_s) \cdot \delta(\Omega_v,\Omega_v^*),$$

Ω_c is the vertical vector unit.

In fact, the expressions of source vectors $[W_{\text{scat}}(\Omega_v), W_{nf}(\Omega_v), W_p(\Omega_v)]$ scattered by a water cell depend on the iteration order:

Iteration k = 1:

$$W_{nf,\text{scat}}(\Omega_v) = W_{\text{scat}}(\Omega_v),$$

$$W_{\text{scat}}(\Omega_v) = \left\{(\rho_w / \pi) \cdot |\Omega_v \cdot \Omega_c| \cdot [1 - R_s^2(n,\theta_s)] \cdot \Delta\Omega_v + R_s^2(n,\theta_s) \cdot \delta(\Omega_v,\Omega_v^*)\right\} \cdot \sum_{o=1}^{\infty} W_{\text{in}}(0,\Omega_s(o)),$$

$$W_p(\Omega_v) = R_p^2(n,\theta_s) \cdot \delta(\Omega_v,\Omega_v^*) \cdot \sum_{o=1}^{\infty} W_{\text{in}}(0,\Omega_s(o)).$$

Iteration k > 1:

$$W_{nf,\text{scat}}(\Omega_v) = \sum_{o=1}^{\infty} nf_{in}(\Omega_{n(o)}) \cdot W_{\text{scat}}(\Omega_{n(o)} \rightarrow \Omega_v),$$

$$W_{\text{scat}}(\Omega_v) = \sum_{o=1}^{\infty} \left\{(\rho_w / \pi) \cdot |\Omega_v \cdot \Omega_c| \cdot [1 - R_s^2(n,\theta_{n(o)})] \cdot \Delta\Omega_v + R_s^2(n,\theta_{n(o)}) \cdot \delta(\Omega_v,\Omega_v^*)\right\} \cdot W_{\text{in}}(0,\Omega_{n(o)}),$$

$$W_p(\Omega_v) = 0.$$

Radiation that has penetrated a water cell and that is not scattered upwards is assumed to be absorbed.

In short, it appears that for all types of cells:

- When a source vector is transmitted without interception through a cell the foliar, nonfoliar and polarization quantities $df(\Omega)$, $nf(\Omega)$, and $p(\Omega)$ of the incident and transmitted source vectors are kept constant. Only, scattering occurring within leaf cells can modify the foliar $df(\Omega)$ and nonfoliar $nf(\Omega)$ coefficients (Table 1).
- Simulation of cell scattering processes does not take into account the actual polarization state of the intercepted radiation. This simplification leads to important computation time reductions. Indeed, exact computations would require to deal with 4×4 Muller matrices (Coulson, 1988) for each directional scattering, instead of two real scattering coefficients $T(\Omega_s,\Omega_v)$ and $T_p(\Omega_s,\Omega_v)$.

ACCELERATING TECHNIQUES

The DART model solves the radiative transfer equation within 3-D covers through iterations on scattering sources. Convergence of this iterative process is slow in optically deep media where components have large single scattering albedos. This is typically the case of radiative transfer in dense forest canopies in the near-infrared domain. Photons can experience many scattering mechanisms before they are absorbed or exit the scene. Thus, radiation transport simulation in large scenes with a large number of discrete directions can lead to tremendous computation times. The DART model allows the operator to select two simple accelerating techniques for reducing these computation times.

Table 1. Changes of the Foliar Diffuse (*df*) and Nonfoliar (*nf*) Components of an Incident Source Vector Scattered by Leaf, Soil, Trunk, and Water Cells.

	Leaf / grass	*Soil*	*Trunk*	*Water*
Foliar diffuse (*n*)	$df_{out} \neq df_{in}$	$df_{out} = df_{in}$	$df_{out} = df_{in}$	$df_{out} = df_{in}$
Nonfoliar diffuse (*df*)	$nf_{out} \neq nf_{in}$	$nf_{out} = nf_{in}$	$nf_{out} = nf_{in}$	$nf_{out} = nf_{in}$

Gauss Seidel Approach

For any iteration $k>1$, the information content of any nonempty cell i comprises the so-called $C_{lm}(i,k)$ and $C_{lm,nf}(i,k)$ coefficients. The operator has the possibility to decide that these coefficients are computed only with source vectors scattered in the $(k-1)$th iteration, or with the help of any relevant source vectors that have been scattered by cells already processed in the $(k-1)$th or the kth iteration order. So, we use updated values of C_{lm} as soon as they become available. The summation of C_{lm} coefficients is done "in place" instead of being "copied" from an earlier iteration to a later one. This approach, called the Gauss-Seidel method, requires a smaller number of iterations for converging. Moreover, it allows one to simulate more accurately 3-D radiative transfer because at each iteration order fluxes are more important and consequently tend to be larger than the selected threshold value ($T_2\langle\sum W\rangle_{1,2}\cdot\Omega_n/4\pi$). This explains why the Gauss-Seidel method tends to give results that are slightly larger than those computed without this approach. The usefulness of this approach was very well verified with simulations. For example, with a homogeneous foliage cover (LAI = 2; $\tau_f=\rho_f=0.45$; spherical LAD; $\rho_{soil}=0.5$; $\theta_s=150°$), without any atmospheric illumination, source vectors computed in the fourth iteration with the Gauss-Seidel method are already more or less equal to those computed in the sixth iteration without the Gauss-Seidel method (Fig. 6). The advantage of the Gauss-Seidel method is even more important with increasing iteration orders. Depending on the number of iterations selected and on the number of iterations that are actually necessary for obtaining a good accuracy, the Gauss-Seidel method can lead to computation time reductions as large as 50%. The only drawback is that it mixes all scattering orders; that is, the different scattering orders cannot be discriminated any more. However, it must be noted that even without the Gauss-Seidel method radiation scattered at iteration k does not correspond exactly with the kth-order scattering because it contains cell multiple scattering.

Reduction of Spherical Harmonics Expansion with Scattering Order

Naturally, radiation scattered by cells is more or less isotropic depending on the LAD of leaf covers. For example, DART simulations applied to homogeneous covers with spherical and planophile LAD showed that the coefficient of variation of specific intensities scattered from individual cells is equal to 10^{-2} and 10^{-1}, respectively, at all scattering orders. On the other hand, the intensity of cell scattered radiation becomes increasingly smaller with larger scattering orders. So, the number of coefficients C_{lm} can be decreased with the iteration order. With computation time being positively correlated to the number of coefficients C_{lm}, smaller numbers of C_{lm} imply shorter computation times. This approach was validated with a number of simulations.

For example, with homogeneous covers characterized by lambertian leaves and different LAD, LAI, and ρ_{soil}, we determined for each iteration order the exact angular distribution of scattered source vectors and specific intensities, the associated C_{lm} coefficients, and the reconstructed angular distribution of scattered source vectors and specific intensities. Each time we considered spherical harmonics expansions of order 0, 1, 2, 3, and 4, that is, 1, 4, 9, 16, and 25 C_{lm} coefficients. In the case of spherical LAD, a spherical harmonics expansion of order 0 starting from the second iteration leads to a relative error, compared to the mean 3-D propagating radiation, less than 1.5% in the near-infrared region ($\rho+\tau=1$) and less than 0.15% in the visible region ($\rho+\tau=0.1$). Leaf cells with planophile LAD lead to more anisotropic distributions of scattered radiation than leaf cells with spherical LAD. Thus, the

Figure 6. DART simulated nadir reflectance of an homogeneous foliar canopy (spherical LAD, $\omega_d=0.9$, $\omega_s=0$, LAI = 2, $\rho_s=0.3$) with iteration order k; $\theta_s=150°$ and no atmopheric irradiance. Crosses indicate simulations (a) without Gauss Seidel (NGS) and (b) with Gauss Seidel (GS). Lines show the exponential curves ($R=A-B\cdot e^{-C\cdot k}$). that fit the NGS case with the second, third, and fourth iterations.

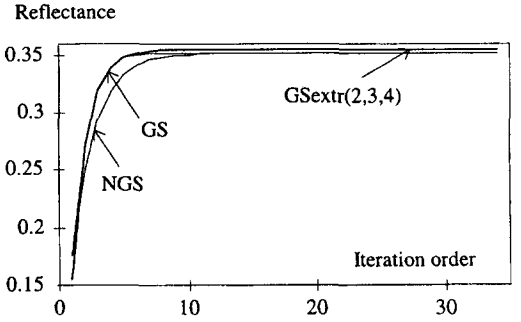

order of spherical harmonics expansion must be larger. An order 2 is a good trade-off; it generates a relative error less than 0.6% in the visible region.

In the case of soil surfaces the expansion order must be at least equal to 4, or even larger, depending on the soil anisotropic characteristics. This number is greatly reduced if the C_{lm} coefficients are computed once the transfer matrix is extended to the forward hemisphere, as mentioned in the previous section. For example, with lambertian soils we selected an order 2, similarly to the case of leaf cells with planophile LAD. Naturally, the order of the spherical harmonics expansion is expected to increase with the presence of strongly anisotropic scattering surfaces and with heterogeneous covers. A number of simulations clearly showed that the decrease of the order of the spherical harmonics expansion allows important computation time reductions; for example, a decrease from 16 to 4 C_{lm} coefficients reduces computation time by a factor 3.

Simulations showed that radiation values tend to converge exponentially with the iteration order, both with the homogeneous covers (Fig. 6) and heterogeneous covers. Thus, convergence values of 3-D absorbed and reflected source vectors are assessed with an exponential extrapolation. This allows us to avoid the computation of unnecessary iteration phases. Denoting A as the convergence value, the analytical extrapolation function is $(A - B \cdot e^{-C \cdot k})$, where k is the iteration order and A, B, and C are unknowns computed with the last three computed iteration orders. A number of simulations were conducted in order to determine the lower three consecutive iterations that lead to accuracy levels better than $5 \cdot 10^{-3}$. It was shown that the set of iterations 2, 3, and 4 fulfills this requirement. In the spectral domains where scene elements have large single scattering albedos, this approach leads to reductions of computation times at least larger than 50%.

PRELIMINARY RESULTS AND DISCUSSION

BRDF Simulations

A number of successful simulations were conducted in order to test the consistency of the DART model. It was verified that simulated BRDF values are constant when the dimensions of the cell matrix (e.g., 16 × 16 × 16 or 200 × 200 × 40 cell matrices) and / or the number of discrete directions (e.g., 288 or 150 directions) are modified, provided, that these numbers are sufficiently large for avoiding side effects that may originate from the space and angular discretization scheme. For example, such effects arise when contiguous cells have large LAI values because within cell exit distances from middle point M_s tend to be smaller along directions around the retroillumination direction. Thus, it results that the single and multiple scattering source vectors tend to be overestimated in the directions around the retroillumination direction.

Homogeneous Spherical Covers

The DART model accuracy was first tested with simulations realized with the SAIL model of Verhoef (1984). This model deals with horizontal homogeneous canopies with leaves characterized by hemispheric reflectance and transmittance. Considering the hypothesis of isotropic upward and downward fluxes of the SAIL model, DART simulations were conducted with homogeneous leaf covers the LAD of which is spherical. A large number of configurations (i.e., variable numbers of discrete directions and cells, sun directions, presence / absence of atmosphere, and optical canopy properties) were tested.

Figure 7 displays DART and SAIL bidirectional reflectance factors in the incidence plane, in the case of a plane homogeneous leaf canopy in the visible ($\rho_d = \tau_d = 0.05$) and the near-infrared ($\rho_d = \tau_d = 0.45$). The reflectance of the underlying soil layer is $\rho_s = 0.15$ and the sun zenith angle is 150°. One hundred fifty unequally spaced discrete directions are selected. Convergence is reached after 10 iterations; only 4 iterations are computed with the Gauss–Seidel method. SAIL and DART simulations agree closely in the visible. The small differences around the hot spot direction are due to the fact that the hot spot effect is more accurately simulated in the DART model; that is, its influence is not considered only along the exact antisolar direction but also around this direction. On the other hand, DART simulations are 3% larger than SAIL simulations in the near-infrared. Larger differences are noted for larger viewing angles. A simplifying assumption of the SAIL model explains these differences. Indeed, this model assumes that hemispheric radiation is isotropic. This is not true, especially for large viewing angles. For example, with the experimental conditions mentioned above, the summation of all upward radiances is larger than the upward hemispheric flux, which means that the latter is underestimated, which in turn implies that SAIL simulations are slightly underestimated. These differences are not noted in the visible because in this spectral domain upward radiation is essentially due to single scattering processes; that is, the upward and downward hemispheric fluxes have relative small values.

The importance of an accurate simulation of within cell scattering was clearly verified with simulations. Indeed, the use of the source vector $\mathcal{W}_1(\Delta l_i, \Omega_s \rightarrow \Omega_v)$ instead of the actual source vector $[W_1(\Delta l_i, \Omega_s \rightarrow \Omega_v) + W_M(\Delta l_i, \Omega_s \rightarrow \Omega_v)]$ may lead to errors as large as 20%. Large errors are obtained with cells with large dimensions and large densities of highly scattering elements.

Heterogeneous Covers

Simulations were also conducted with heterogeneous 3-D artificial scenes, for example, scenes with groups

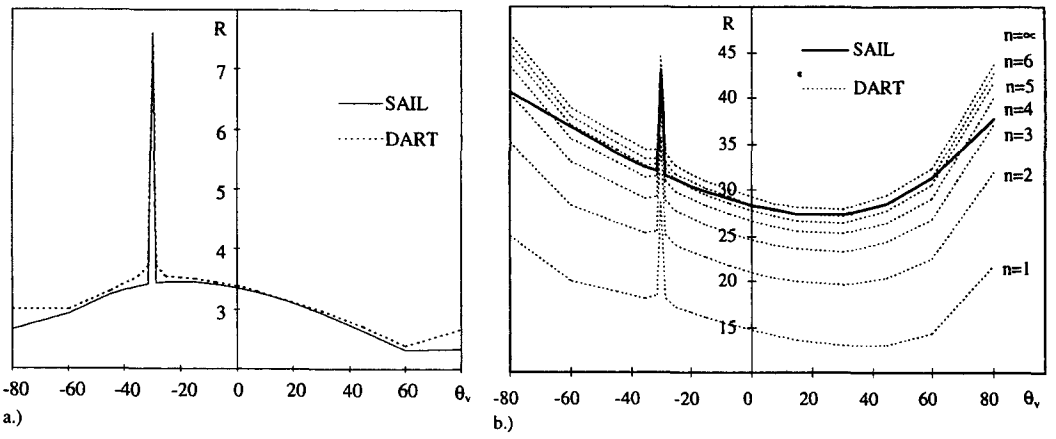

Figure 7. Comparison of DART (20 layers of leaf cells) and SAIL simulated reflectances (R) in the incidence plane of an homogeneous cover (LAI = 2; spherical LAD; $\theta_s = 150°$; $\rho s = 0.15$). a.) $\rho_d = \tau_d = 0.45$; b.) $\rho_d = \tau_d = 0.05$. Iterations $n = 1$ to $n = 6$ and the extrapolated iteration ($n = \infty$) of DART simulations are shown.

of trees surrounded by grass. Naturally, computer times simulations are all the more important than the numbers of discrete directions and non empty cells are large; for example, a $200 \times 200 \times 30$ cell matrix and a $100 \times 100 \times 30$ cell matrix with the same number of "nonempty" cells lead to similar computation times. The DART model provides three types of results: 1) mean scene BRDF (Fig. 8) or mean BRDF of any set of pixels of the top scene, 2) directional spectral images (Fig. 9), that is, simulation of remotely acquired acquisitions, and 3) 3-D description of intercepted and absorbed radiation within the scene.

Figures 8a and 8b show the simulated near infrared BRDF of an homogeneous and heterogeneous tree cover, with the same LAI. They are displayed in a rectangular coordinate system ($x = k \cdot \theta \cdot \cos \varphi$, $y = k \cdot \theta \cdot \sin \varphi$) where θ and φ are the zenith and azimuth viewing directions. The heterogeneous scene was simulated with an algorithm developed by Pinel et al. (1995). Trees comprise a trunk and an ellipsoidal crown. Their position is spatially random, whereas tree height, crown width, and crown height vary randomly around mean values. Moreover, crowns can be randomly filled with leaf cells for simulating foliar clumping. It is well verified that the hot spot occurs where the viewing and solar zenith angle coincide, that is, where shadows are concealed. It was verified that the shape of the BRDF is directly related to tree density and to the amount of mutual shadowing that is taking place. The BRDF's bowl that occurs when the viewing angle moves opposite the sun zenith angle, in the case of the homogeneous cover, tends to disappear with the heterogeneous cover. Moreover, the heterogeneous cover leads to smaller BRDF values.

Figure 8. Simulated BRDF of a an homogeneous and b a heterogeneous scene: leaf canopy (LAI = 1.17, $\rho_d = \tau_d = 0.05$, $\omega_s = 0$, spherical LAD), grass (LAI = 3, $\rho_d = \tau_d = 0.05$, $\omega_s = 0$, spherical LAD), soil ($\rho_{soil} = 0.1$), $\theta_s = 150°$, $\varphi_s = 45°$. Mean characteristics of the heterogeneous scene are: tree density (164 trees / ha), tree height (20 ± 3 m), crown height (12 ± 1 m), crown width (6 ± 1 m) and trunk diameter (40 ± 5 cm).

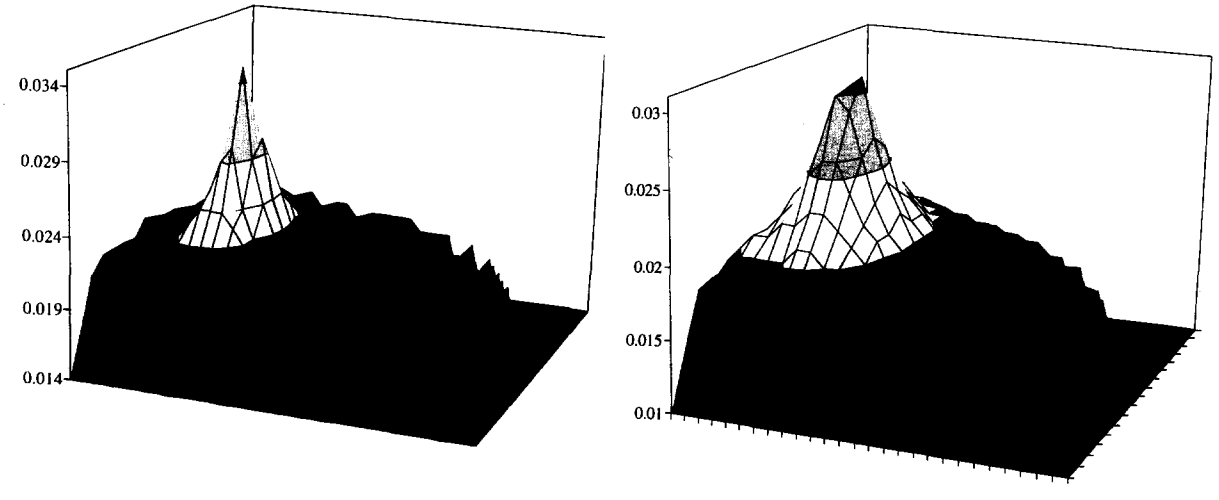

Comparison with Remotely Acquired Images

A study was also started for testing the DART model with 1.60-m resolution data acquired with an airborne SPOT HRV simulator above a pine plantation located in Les Landes forest, southwest France. This is a large, flat homogeneous forest of 1 million hectares, producing 20% of French timber, mainly maritime pine (*Pinus pinaster*). The test area encompasses several thousand hectares that comprise several hundred large forest stands (mean area of 20 ha), are rectangular in shape, and are delimited by fire protection tracks or large access tracks. Characteristics (i.e., row spacing and width, tree density, dbh, canopy depth, understory vegetation, etc.) of the stands of maritime pine are well documented (Gastellu-Etchegorry et al., 1995).

Measurements in the field, at the time of the airborne acquisitions, of pine parcels optical and structural characteristics allowed us to obtain realistic models of a few parcels. Figures 9a–h show DART simulated reflectance images in the visible domain of a 52-year-old pine stand of the Landes forest, France. All simulations are with a direct sun illumination ($\theta_s = 143°\varphi_s = 135°$) except simulation of Figure 9c, which is with atmosphere irradiance only. Major characteristics of the scene are listed below:

- Crowns: ellipsoidal shape, LAI = 3, spherical LAD, width = 6 ± 1 m, $\rho_d = \tau_d = 0.05$, $\omega_s = 0$, crown height = 12 ± 1 m, tree height = 20 ± 3 m.
- Trunks: density = 164 trees / ha, diameter = 40 ± 5 cm, $\rho_{trunk} = 0.06$.
- Grass: LAI = 1.5, spherical LAD, $\rho_d = \tau_d = 0.08$.
- Soil: flat. $\rho_d = 0.06$.

A nadir image ($\theta_v = 0°$) is shown in Figure 9a. The absence of atmosphere radiation ensures that shadows of tree trunks and tree canopies appear clearly. These shadows are orientated along the illumination azimuth angle, that is, 135°. The low LAI of the tree canopy explains why the superposition of shadows gives rise to shadows with different gray tone levels. This explains also why canopies are more or less bright, depending on the illumination conditions and optical characteristics of the background objects along the viewing direction. Parts of crowns that are directly illuminated are brighter due to larger reflectances; that is, 0.025 instead of 0.007. The brighter tone of ground surface indicates a larger reflectance value (0.028). Figure 9b is associated with the ($\theta_v = 16°$; $\varphi_v = 180°$) viewing direction. Then, the base of the trunks can be seen. We can note that, compared to Figure 9a, the shadows of trunks and crowns do not appear at the same positions. This change with the viewing direction is simply explained by the fact that the ground surface is much below the upper level of the scene. Moreover, the mean scene reflectance increased by 22% (Table 2). This is essentially due to the combination of a decrease of the shadow surface and to a lesser extent to a 10% increase of grass reflectance with larger viewing zenith angles. Thus, the canopy structure explains that the scene reflectance increases more with the zenith viewing angle that the reflectance of an homogeneous layer such as the understory. Figure 9c is associated with the same viewing direction as Figure 9b, but without direct sun illumination, that is, SKYL = 1. Thus shadows do not appear. In fact, low contrast shadows are observed with simulations conducted with incident anisotropic atmosphere radiation.

Figure 9d shows a simulated directional image with a ($\theta_v = 58°;\varphi_v = 0°$) viewing direction. The larger viewing zenith angle explains the larger proportion of apparent crowns and the smaller apparent surface of shadows and illuminated ground. The combination of these variations explains a small 3% decrease of the scene reflectance from $\theta_v = 16°$ to $\theta_v = 58°$ compared to the associated 7% increase of the mean reflectance of the understory. Once more, the structure of the forest cover is responsible of this anisotropic and irregular behavior of the scene BRDF. Undoubtedly the understory displays a more consistent directional behavior: Its reflectance increases steadily from 0.028 to 0.033 with viewing zenith angles from 0° to 58°. This effect is even amplified with vertical sun illumination (simulations not shown here). Indeed, compared to the ($\theta_s = 143°$; $\varphi_s = 135°$) illumination condition nadir scene reflectance is much larger (i.e, 0.22 instead of 0.013) due to the absence of shadows, whereas it is about the same (i.e., 0.015) with the 58° zenith viewing angle.

Figure 9e shows a simulated directional image with a ($\theta_v = 37°$; $\varphi_v = 45°$) viewing direction. Shadows of trunks are oriented along the azimuthal illumination direction (i.e., 135°). They are perpendicular to the trunk axes, which are oriented along the azimuthal viewing direction. The small percentage of illuminated ground surface, the nonnegligible shadow extent, and the relatively small reflectance value of crowns explain the low value (i.e., 0.0124) of the scene reflectance. Figure 9g represents a directional image in the so-called hot spot configuration (i.e., $\theta_v = 37°$; $\varphi_v = 315°$). The absence of shadow is clearly verified whereas grass and crowns have their maximum reflectance values, 0.044 and 0.024, respectively. These two effects explain that the scene has its larger reflectance value in that viewing configuration. This is more or less twice the nadir scene reflectance, that is, 0.029 instead of 0.013. This configuration is undoubtedly potentially important for studying canopy structure because the scene reflectance value is strongly dependent on the size, shape, and density of the tree cover. This point is of special importance with the advent of directional satellite sensors such as POLDER (Deschamps et al., 1994).

The 2-D images (Figs. 9b, 9c, 9e, and 9g) of the

Table 2. Mean Illuminated Grass, Illuminated Crown, and Scene Reflectance Values.

	$\theta_v = 0°$	$\theta_v = 16°$, $\varphi_v = 0°$	$\theta_v = 37°$, $\varphi_v = 45°$	$\theta_v = 37°$, $\varphi_v = 315°$	$\theta_v = 58°$, $\varphi_v = 0°$
Grass	0.028 (17%)	0.031 (17%)	0.029 (6%)	0.044 (28%)	0.033 (5%)
Crown	0.015 (46%)	0.017 (61%)	0.014 (74%)	0.024 (69%)	0.017 (80%)
Scene	0.013	0.0158	0.0124	0.029	0.0153

[a] Ground cover of illuminated grass and illuminated crowns are shown between brackets.

reflectance factors $R(\Omega_v)$ of the upper cells of the scene are not actual simulations of images that a sensor above the canopy would acquire with an (Ω_v) viewing direction. Indeed simulations of remote sensing acquisitions correspond to the projection of the upper cells reflectance factors $R(\Omega_v)$ onto a plane perpendicular to the viewing direction (Ω_v). For example, geometrically corrected simulations of Figures 9f and 9h are the projections of images of Figures 9e and 9g. Rectangular scenes are transformed into lozenges the size of which depends on the viewing direction. It should be noted that the dimensions of the images of Figures 9d, 9f, and 9h were vertically enlarged in order to fit with the other images.

Preliminary analyses of the remotely acquired image at hand showed that from a statistical point of view the image simulated with clear sky conditions (Fig. 9a) compares very well with this remote sensing image; that is, it presents similar radiometric and textural information characteristics. This clearly stresses the potential of the DART model for studying vegetation with remote sensing information.

CONCLUSION AND PERSPECTIVE

The DART model was developed in order to simulate radiative transfer, and consequently BRDF, in heterogeneous 3-D scenes, with two complementary objectives in mind: 1) to investigate and better model the potential information in remote sensing data about biophysical and biochemical characteristics of vegetation covers, and 2) to develop a model that could provide useful information for further vegetation functioning studies.

This model can be used as an efficient tool for improving our understanding and interpretation of remotely acquired data, for example, better determination of the albedo of earth surfaces. It can work with scenes that comprise different types of elements (leaves, grass, soil, water, and trunks), with any 3-D distribution. Topography is simulated. Major physical mechanisms (e.g., polarization, heterogeneous atmospheric irradiance, and hot spot) are considered. The simulation of polarization is achieved without taking into account the polarization state of incident radiation. Only single scattering polarization mechanisms are modeled. Scalar summation of polarized radiation is performed under a drastic assumption: Single scattered radiation is assumed to have the same polarization direction. This is undoubtedly an oversimplifying assumption which is used only in order to give a rough estimate of the polarization degree of scattered radiation. The number and orientation of discrete directions and the space discretizing scheme are selected by the operator. Cells can have different dimensions along the *Ox*, *Oy*, and *Oz* axes. This possibility, combined with an accurate simulation of within cell scattering, is aimed to simulations of large size scenes. The model is statistical when dealing with foliage within individual leaf and grass cells, but deterministic when dealing with the shape and spatial distribution of the objects that make up the scene. The deterministic approach plays an essential and straightforward role for obtaining accurate simulations of radiative transfer in 3-D heterogeneous scenes. An important advantage of the DART model is to distinguish radiation components that comprise and do not comprise leaf volume information. This is of special importance for studying the biochemistry of vegetation covers with remotely acquired data. Finally, the possibility of providing realistic simulations of remotely acquired directional spectral images is a major highlight of the DART model, for remote sensing based studies, especially when we want to determine from remote measurements the spatial distribution of biophysical and biochemical characteristics of vegetation covers.

In a first series of tests the DART model was successfully validated against the SAIL model, in the case of homogeneous covers with spherical LAD. Different configurations (sun and viewing directions, canopy optical and structural properties, and dimensions of the scene) were tested. Encouraging results were also obtained with other series of tests that were conducted with heterogeneous covers. Naturally, these preliminary tests should be pursued for a full validation of the DART model. In this context, two complementary approaches are being implemented. First, it will be conducted analyses of model sensitivity to the input parameters (optical, structural, and biological). Second, forward model calculations will be compared with 1) laboratory and field BRDF measurements of natural and artificial targets, such as directional PARABOLA data (Deering et al., 1994) and 2) directional and polarization airborne data acquired by the POLDER instrument (Deschamps et al., 1994) in the frame of the BOREAS project (Sellers et al., 1993).

A major objective of remote sensing studies is to obtain quantitative information on the spatial and temporal distribution of biophysical and biochemical charac-

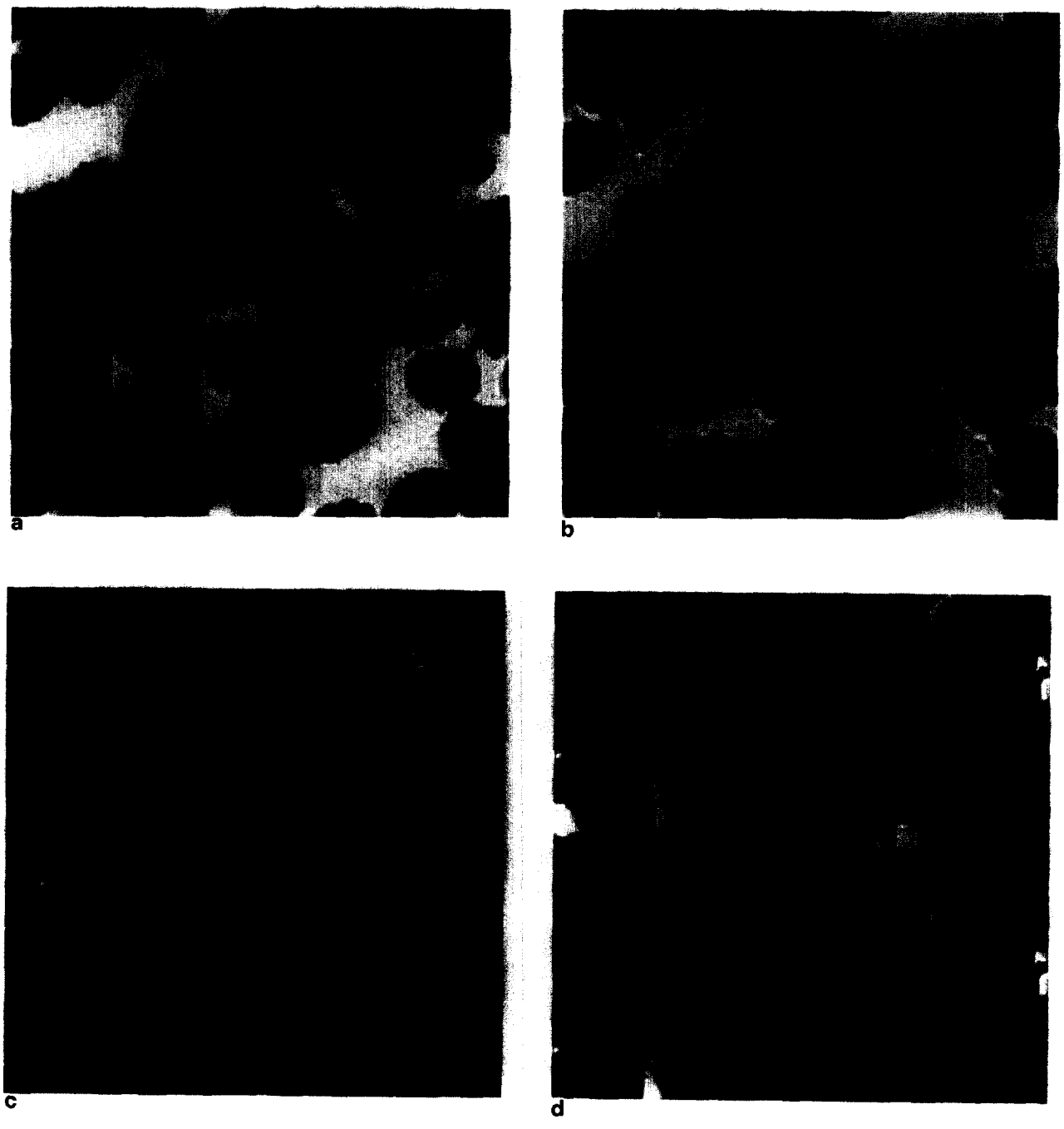

Figure 9. DART simulated directional images in the visible domain of a 52-years-old pine stand: a): $\theta_v = 0°$, b) and c) $\theta_v = 16°$ and $\varphi_v = 0°$, d): $\theta_v = 58°$ and $\varphi_v = 0°$, e) and f): $\theta_v = 37°$ and $\varphi_v = 45°$, g) and h) $\theta_v = 37°$ and $\varphi_v = 315°$. d), f) and h) are geometrically corrected simulations. Sun direction is ($\theta_s = 143°$;$\varphi_s = 135°$) except for c) where SKYL = 1. A 100 × 100 × 50 cell matrix was used with 120 discrete directions. Canopy characteristics are mentioned in the text.

teristics of vegetation. These characteristics are critical inputs to ecological models that describe the interaction between the land surface and climate, energy balance, and hydrologic and biochemical cycles (Wu and Stralher, 1994). In this context, we intend to use the DART model to investigate the capability of remote sensing, first with forward simulations applied to large areas and second with inversion techniques. Naturally, realistic simulations of the BRDF of large heterogeneous areas require important simplifying hypotheses. For example, the number of individual cells must be necessarily limited in order to limit computational expenses. Thus, with large areas, although the number of cells is kept to an acceptable value, the representation of the optical properties of the individual cells may become more and more complex to compute and to handle. In fact, the DART model was designed to overcome this situation in a simple manner. The first step involves the

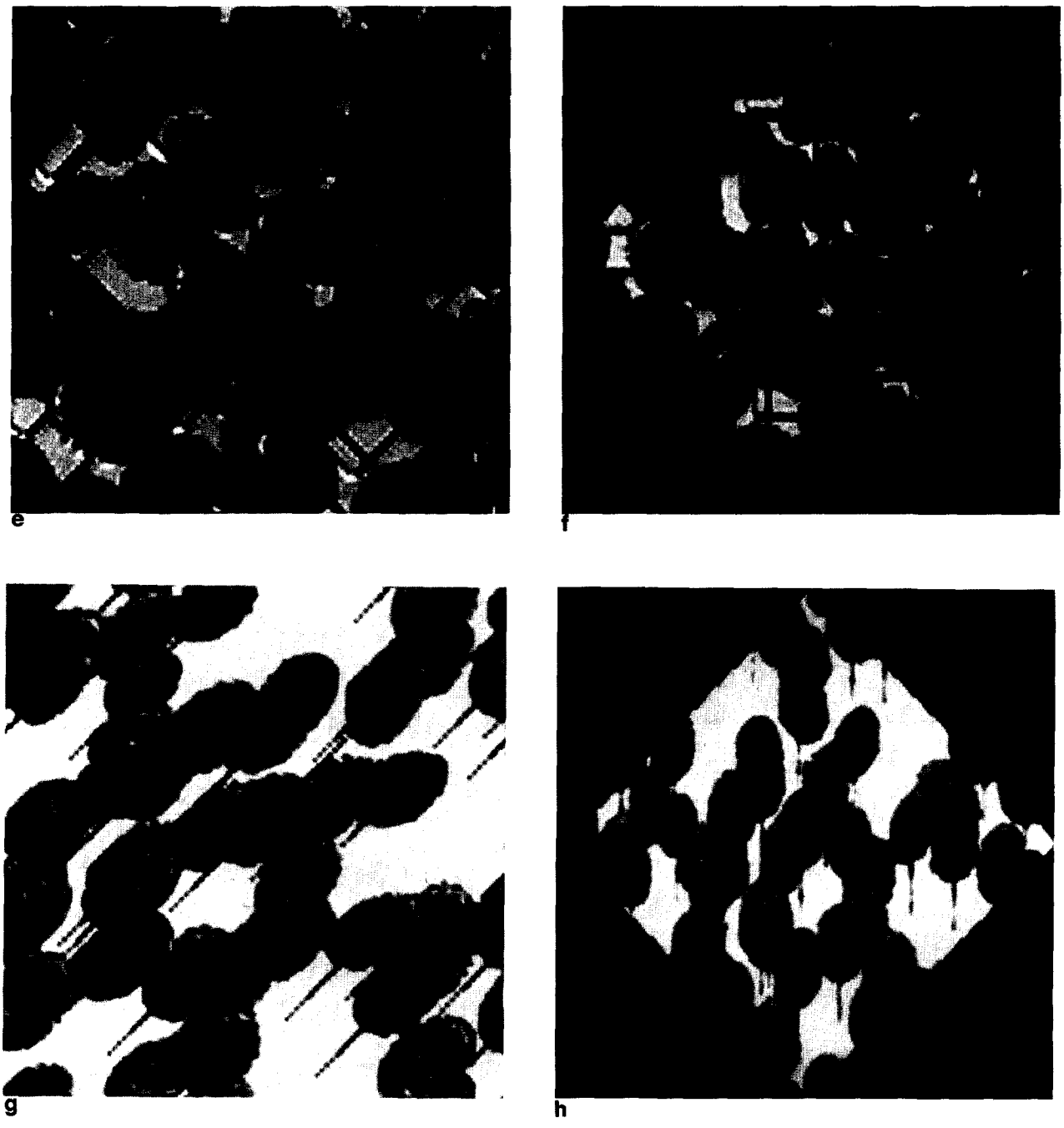

Figure 9. (continued)

use of a find grid mesh scene with the computation of the so-called macroscopic optical characteristics, that is, essentially the scattering phase function and the directional transmission function, of primitive 3-D elements such as tree crowns. The latter are described by sets of contiguous cells, possibly with different optical and structural characteristics. Then, in a second step, these macroscopic characteristics are used as input parameters associated with individual cells of the scene that is simulated with a large grid mesh. This approach allows us to deal with large scenes. It will be presented in a forthcoming article. It provides a physical background for investigating the so-called problem of spatialization of information that is typically met in the frame of remote sensing studies conducted with sensors that operate with different ground resolutions.

The inversion of reflectance models with remote sensing data requires both sound atmospheric corrections and the use of a necessarily limited set of input parameters, that is, unknowns that describe the scene. In the case of the DART model, the number of input parameters can be greatly reduced through simple ap-

proximations. For example, the DART model can be operated with a scene that is simulated with a limited set of input parameters such as "tree height, ground cover, LAI, LAD, $\rho_{d,\text{leaf}}$, $\tau_{d,\text{leaf}}$, atmospheric irradiance, sun irradiance, and ρ_{ground}," with a random spatial distribution of vegetation elements (Pinel et al., 1995). In this context, we plan to test ordinary inversion approaches, that is, optimum techniques to invert directional data through minimizing a merit function consisting of the sum of the squares of the residuals and a penalty function. To date, according to Liang and Stralher (1993), the most successful direct search algorithm is the method of Powell (1964), especially with the modifications suggested by Zangwill (1967) and Brent (1973), because it does not require computation of the derivatives of the merit function. Another inversion approach will be also investigated by the authors: fitting of simulations, conducted while varying a limited set of input parameters, with invertible mathematical expressions such as the statistical BRDF expressions of Liang and Stralher (1993).

In addition to the above-mentioned validations and investigations, we plan also to use the DART model for conducting research works in the two following domains:

- Biochemical investigations: Determination of the percentage of information specific to leaf interior in remote sensing acquisitions. This is possible because the DART model uses different transfer functions for leaf volume and surface scattering mechanisms. These functions may be computed by the model or simply used as input parameters, without any limiting hypothesis concerning their rotational invariance. The distinction between foliar and nonfoliar information is essential for assessing the actual potential of remote sensing for studying the chemistry (e.g, chlorophyll and nitrogen content) of vegetation (Gastellu-Etchegorry et al., 1995) from space. For example, direct DART simulations allow us to access to which extent the canopy geometry confounds extraction of foliar information.
- Physiological investigations: Vegetation functioning can be studied through the coupling of the DART model with leaf physiological models such as the three-parameter model of Johnson and Thornley (1984) or the semiempirical mechanistic model of leaf photosynthesis and stomatal conductance of Collatz et al. (1991). Thanks to the determination of the 3-D distribution of photosynthetically active radiation (PAR) absorbed by vegetation, this approach leads to an assessment of the photosynthetic efficiency of vegetation covers.

The authors wish to thank Miss Marie Pierre Rocca for her valuable contribution in this work. Moreover, this research would not have been possible without the financial support of the Centre National pour la Recherche Scientifique (CNRS), the IGBP (France) Ecosystems Program (Temperate Forests), and the Centre National d'Etude Spatiale (CNES). We want also to thank the reviewers for their useful and encouraging comments.

REFERENCES

Barker Schaaf, C., and Stralher, A. H. (1994), Validation of bidirectional and hemispherical reflectances from a geometric-optical model using ASAS imagery and pyranometer measurements of a spruce forest. *Remote Sens. Environ.* 49:138–144.

Borel, C. C., Gerstl, S. A. W., and Powers, B. J. (1991), The radiosity method in optical remote sensing of structural 3-D surfaces. *Remote Sens. Environ.* 36:13–44.

Brent, R. P. (1973), *Algorithms for Minimizing without Derivatives*, Prentice-Hall, Englewood Cliffs, NJ.

Collatz, G. J., Ball, J. T., Grivet, C., and Berry, J. A. (1991), Physiological and environmental regulation of stomatal conductance, photosynthesis and transpiration: a model that includes a laminar boundary layer, *Agric. For. Meteorol.* 54:107–136.

Coulson, K. L. (1988), *Polarization and Intensity of Light in the Atmosphere*, Deepak, Hampton, VA.

Dave, J. V. (1978), Extensive datasets of the diffuse radiation in realistic atmospheric models aerosols and common absorbing gases, *Solar Energy* 21:361–369.

Deering, D. W., Middleton, E. M., and Eck, T. F. (1994), Reflectance anisotropy for a spruce-hemlock forest canopy, *Remote Sens. Environ.* 47:242–260.

Deschamps, P. Y., Bréon, F. M., Leroy, M., et al. (1994), The POLDER mission; Instrument characteristics and scientific objectives, *IEEE Trans. Geosci. Remote Sens.* 32:598–614.

Egan, W. G. (1985), *Photometry and Polarization in Remote Sensing*, Elsevier, Amsterdam.

Gao, W. (1993), A simple bidirectional reflectance model applied to a tallgrass canopy, *Remote Sens. Environ.* 45: 209–224.

Gastellu-Etchegorry, J. P., Demarez, V., Pinel, V., and Zagolski, F. (1994), Modeling radiative transfer in heterogeneous 3D vegetation canopies, in *Proceedings EUROPTO of the International Symposium on Satellite Remote Sensing*, Rome, Italy, SPIE Vol. 2314, pp. 38–49.

Gastellu-Etchegorry, J. P., Zagolski, F., Mougin, E., Marty, G., and Giordano, G. (1995), An assessment of canopy chemistry with AVIRIS—a case study in the Landes forest, France, *Int. J. Remote Sens.* 16(3):487–501.

Gastellu-Etchegorry, J. P., Zagolski, F., and Romier, J. (1996), A simple anisotropic reflectance model for homogeneous multilayer canopies, *Remote Sens. Environ.*, 57:22–38.

Hapke, B. (1993), *Theory of Reflectance and Emittance Spectroscopy*, Topics in Remote Sensing, Vol. 3, Cambridge University Press, Cambridge.

Jessel, J. P. (1992), Modélisation par réseaux d'atomes pour la représentation d'objets et pour l'illumination globale. Ph.D. thesis, Paul Sabatier University.

Johnson, I. R., and Thornley, J. H. M. (1984), A model of instantaneous and daily canopy photosynthesis, *J. Theor. Biol.* 107:531–545.

Kimes, D. S. (1991), Radiative transfer in homogeneous and heterogeneous vegetation canopies, in *Photon-Vegetation Interactions* (R. B. Myneni and J. Ross, Eds.), SpringerVerlag, Berlin, Heidelberg, New York, pp. 339–388.

Kimes, D. S., and Kirchner, J. A. (1982), Radiative transfer model for heterogeneous 3-D scenes, *Appl. Opt.* 21:4119–4129.

Kimes, D. S., and Sellers, P. J. (1985), Inferring hemispherical reflectance of the Earth's surface for global energy budgets from remotely sensed nadir or directional radiance values, *Remote Sens. Environ.* 18:205–223.

Kimes, D. S., Newcomb, W. W., Schutt, J. B., Pinter, P. J., and Jackson, R. D. (1986), Directional reflectance distribution of a hardwood and pine forest canopy, *IEEE Trans. Geosci. Remote Sens.* GE-24:281–293.

Kuusk, A. (1985), The hot spot effect of a uniform cover, *Sov. J. Remote Sens.* 3(4):645–658.

Liang, S., and Stralher, A. H. (1993), An analytical BRDF model of canopy radiative transfer and its inversion, *IEEE Trans. Geosci. Remote Sens.* 31(5):1081–1092.

Li, X., and Strahler, A. H. (1986), Geometric-optical bidirectional reflectance modeling of a coniferous forest canopy, *IEEE Trans. Geosci. Remote Sens.* GE-24:906–919.

Myneni, R. B., Asrar, G., and Gerstl, A. W. (1990), Radiative transfer in three dimensional leaf canopies, *Trans. Theory Stat. Phys.* 19:1–54.

Myneni, R. B., Marshak, A., Knyazikhin, Y., and Asrar, G. (1991), Discrete ordinates method for photon transport in leaf canopies, in *Photon–Vegetation Interactions* (R. B. Myneni and J. Ross, Eds.), Springer-Verlag, Berlin, Heidelberg, New York, pp. 45–109.

Perraudeau, M. (1988), Distribution de la luminance du ciel, Cahiers du Centre Scientifique et Technique du Batiment 295-2305, Orleans. December.

Pinel, V., Gastellu-Etchegorry, J. P., and Demarez, V. (1995), BRDF simulations of forest covers with the coupling of high and medium resolution reflectance models, in *IGARSS '95*, Firenze, Italy, IEEE publication.

Pinty, B., and Ramond, D. (1986), A simple bidirectional reflectance model for terrestrial surfaces, *J. Geophys. Res.* 91:7803–7808.

Powell, M. J. D. (1964), An efficient method for finding the minimum of a function of several variables without calculating derivatives, *Comput. J.* 7:155–162.

Press, W. H., Teukolsky, A. A., Vetterling, W. T., and Flannery, B. P. (1992), *Numerical Recipes in C, The Art of Scientific Programming*, Cambridge University Press, Cambridge.

Qin, W., and Xiang, Y. (1994), On the hotspot effect of leaf canopies: modeling study and influence of leaf shape, *Remote Sens. Environ.* 50:95–106.

Reyna, E., and Badhwar, G. D. (1985), Inclusion of specular reflectance in vegetative canopy models, *IEEE Trans. Geosci. Remote Sens.* 23(5):731–736.

Rondeaux, G., and Herman, M. (1991), Polarization of light reflected by crop canopies, *Remote Sens. Environ.* 38:63–75.

Sellers, P. J., Hall, F. G., Baldocchi, D., et al. (1993), Boreas, Boreal ecosystem, Atmosphere study, in *Experimental Plan*, Chap. 1–3 (P. J. Sellers, F. G. Hall, D. Baldocchi et al. Eds.)

Suits, G. H. (1972), The calculation of the directional reflectance of a vegetative canopy, *Remote Sens. Environ.* 2:117–125.

Syren, P. (1994), Reflectance anisotropy for nadir observations of coniferous forest canopies, *Remote Sens. Environ.* 49: 72–80.

Vanderbilt, V. C., Grant, L., and Ustin, S. L. (1991), Polarization of light by vegetation, in *Photon–Vegetation Interactions*, (R. B. Myneni and J. Ross, Eds.), Springer-Verlag, Berlin, Heidelberg, New York, pp. 191–228.

Verhoef, W. (1984), Light scattering by leaf layers with application to canopy reflectance modeling: the SAIL model, *Remote Sens. Environ.* 16:125–141.

Walthall, C. L., Norman, J. M., Welles, J. M., Campbell, G., and Blad, B. (1985), Simple equation to approximate the bidirectional reflectance for vegetative canopies and bare soil surfaces, *Appl. Opt.* 24:383–387.

Wu, Y., and Stralher, A. H. (1994), Remote estimation of crown size, stand density, and biomass on the Oregon transect, *Ecol. Appl.* 4(2):299–312.

Zangwill, W. I. (1967), Minimizing a function without calculating derivatives, *Comput. J.* 10:293–296.

APPENDIX: MULTIPLE SCATTERING WITHIN LEAF CELLS

Simulation of multiple scattering within leaf cells does not take into account polarization mechanisms. This is conducted with the computation of the interception (Fig. 4) of $\mathscr{W}_1(\Delta l_i,\Omega_s\rightarrow\Omega_v)$ along the path $\Delta_{Si}(\Omega_v)$:

$$\mathscr{W}_{1,\text{int}}(\Delta l_i,\Omega_s\rightarrow\Omega_v) = [\mathscr{W}_{d1}(\Delta l_i,\Omega_s\rightarrow\Omega_v) - \mathscr{W}_{d1}(\Delta l_i,\Omega_s\rightarrow\Omega_v)] + [\mathscr{W}_{s1}(\Delta l_i,\Omega_s\rightarrow\Omega_v) - W_{s1}(\Delta l_i,\Omega_s\rightarrow\Omega_v)].$$

We have:

$$\mathscr{W}_{nf,1,\text{int}}(\Delta l_i,\Omega_s\rightarrow\Omega_v) = nf_{\text{in}},(\Omega_s)\cdot s_1(j,\Omega_s,\Omega_v)\cdot\mathscr{W}_{1,\text{int}}(\Delta l_i,\Omega_s\rightarrow\Omega_v).$$

Integration over all exit directions (Ω_v) leads to total intercepted energy:

$$\mathscr{W}_{1,\text{int}}(\Delta l_i,\Omega_s) = \sum_{v=1}^{N}\mathscr{W}_{1,\text{int}}(\Delta l_i,\Omega_s\rightarrow\Omega_v) = \left[\sum_{v=1}^{N}(1 - T(\Delta s_i,\Omega_v))\cdot T(j,\Omega_s,\Omega_v)\right]\cdot W_{\text{int}}(\Delta l_i,\Omega_s).$$

In turn, the energy intercepted $\mathscr{W}_{1,\text{int}}(\Delta l_i,\Omega_s)$ leads to scattering mechanisms of order larger than 1, which cannot be modeled exactly. Thus, in a first approximation, radiation that has undergone more than one scattering within a cell is assumed to be nearly isotropic. This allows one to define for cells of type j mean single

scattering albedos ω_{dj} and ω_{sj} associated with diffuse and specular scattering, respectively:

$$\omega_{dj} = \frac{1}{4\pi} \cdot \int_{4\pi} \int_{4\pi} f_d(j,\Omega_f,\Omega_s \rightarrow \Omega_v) \cdot d\Omega_v \cdot d\Omega_s$$

$$= \frac{1}{4\pi} \cdot \sum_{v=1}^{N} \sum_{s=1}^{N} T_d(j,\Omega_s,\Omega_v) \cdot \Delta\Omega_s,$$

$$\omega_{sj} = \frac{1}{4\pi} \cdot \int_{4\pi} \int_{4\pi} f_s(j,\Omega_s \rightarrow \Omega_v) \cdot d\Omega_v \cdot d\Omega_s$$

$$= \frac{1}{4\pi} \cdot \sum_{v=1}^{N} \sum_{s=1}^{N} T_s(j,\Omega_s,\Omega_v) \cdot \Delta\Omega_s.$$

In the case of foliar elements with lambertian and Fresnel scattering phase functions,

$$\omega_{dj} \approx \rho_{dj} + \tau_{dj}$$

and $$\omega_{sj} = \frac{1}{4\pi} \cdot \sum_{s=1}^{N} K_j(\kappa,\psi_{fs}) \cdot R_s^2(n_j,\psi_{fs}) \cdot \Delta\Omega_s.$$

Thus, total mean single scattering albedo of cell i of type j is defined by $\omega_j = \omega_{dj} + \omega_{sj}$.

It results that total multiple-scattering source vector that escapes cell i is

$$W_M(\Delta l_i,\Omega_s) = \mathscr{W}_{1,\text{int}}(\Delta l_i,\Omega_s) \cdot \{\omega_j \cdot \langle T_i \rangle + \omega_j \cdot \langle T_i \rangle \cdot [\omega_j - \omega_j \cdot \langle T_i \rangle] + \omega_j \cdot \langle T_i \rangle \cdot [\omega_j - \omega_j \cdot \langle T_i \rangle]^2 + \cdots\}$$

$$\Rightarrow W_M(\Delta l_i,\Omega_s) \approx \left[\frac{\omega_j \cdot \langle T_i \rangle}{1 - \omega_j \cdot [1 - \langle T_i \rangle]}\right] \cdot \mathscr{W}_{1,\text{int}}(\Delta l_i,\Omega_s),$$

where $\langle T_i \rangle$ is the mean transmission coefficient within cell i. This is assumed to be equal to the transmission coefficient from the center of cell i. With $\Delta m_i(\Omega)$ being the propagation length along direction (Ω) from the center of cell i, we have

$$\langle T_i \rangle = \frac{1}{4\pi} \cdot \int_{4\pi} e^{-G(j,\Omega) \cdot u_f(i) \cdot \Delta m_i(\Omega)} \cdot d\Omega$$

$$= \frac{1}{4\pi} \cdot \sum_{v=1}^{N} [T(j,\Omega_v)]^{u_f(i) \cdot \Delta m_i(\Omega_v)} \cdot \Delta\Omega_v.$$

We can note that if the terms $T(j,\Omega_v)$ are not too much anisotropic or if the cell leaf area density is not much larger than 1, then we have

$$\langle T_i \rangle \approx \langle T_{o,j} \rangle^{u_f(i)} \quad \text{with}$$

$$\langle T_{o,j} \rangle = \frac{1}{4\pi} \cdot \sum_{v=1}^{N} \left[T(j,\Omega_v)\right]^{\Delta m_i(\Omega)} \cdot \Delta\Omega_v.$$

Similarly, the multiply specularly scattered source vector that escapes cell i is

$$W_{sM}(\Delta l_i,\Omega_s) = \mathscr{W}_{1,\text{int}}(\Delta l_i,\Omega_s) \cdot \{\omega_{sj} \cdot \langle T_i \rangle + \omega_{sj} \cdot \langle T_i \rangle \cdot [\omega_{sj} - \omega_{sj} \cdot \langle T_i \rangle] + \omega_{sj} \cdot \langle T_i \rangle \cdot [\omega_{sj} - \omega_{sj} \cdot \langle T_i \rangle]^2 + \cdots\}$$

$$\Rightarrow W_{sM}(\Delta l_i,\Omega_s) \approx \frac{\omega_{sj} \cdot \langle T_i \rangle}{1 - \omega_{sj} \cdot [1 - \langle T_i \rangle]} \cdot \mathscr{W}_{1,\text{int}}(\Delta l_i,\Omega_s),$$

Thus, multiple-scattering radiation associated with at least one leaf volume scattering is

$$W_{dM}(\Delta l_i,\Omega_s) \approx \left[\frac{\omega_j \cdot \langle T_i \rangle}{1 - \omega_j \cdot [1 - \langle T_i \rangle]} - \frac{\omega_{sj} \cdot \langle T_i \rangle}{1 - \omega_{sj} \cdot [1 - \langle T_i \rangle]}\right] \cdot \mathscr{W}_{1,\text{int}}(\Delta l_i,\Omega_s)$$

Multiplicative terms $\frac{\langle T_i \rangle}{1 - \omega_j \cdot [1 - \langle T_i \rangle]}$ are always less than 1, except if $\langle T \rangle = 1$ (i.e., empty cell), or if $\omega_j = 1$ (i.e., no absorption loss). Thus we have

$$W_M(\Delta l_i,\Omega_s) < \omega_j \cdot \mathscr{W}_{1,\text{int}}(\Delta l_i,\Omega_s) \quad \text{and}$$
$$W_{sM}(\Delta l_i,\Omega_s) < \omega_{sj} \cdot \mathscr{W}_{1,\text{int}}(\Delta l_i,\Omega_s).$$

Coefficients $\langle T_{o,j} \rangle$, ω_{dj}, and ω_{sj} depend only on the type of leaf cell, that is, its leaf angle distribution and optical properties. They are computed in the first step of the DART simulation for each type of leaf cell, in order to minimize repetitive computations.

The multiple-scattering source vector $W_M(\Delta l_i, \Omega_s \rightarrow \Omega_v)$ is assumed to be proportional to $W_M(\Delta l_i,\Omega_s)$, to the transmittance along $\Delta s_i(\Omega_v)$ and to the sum of the differential scattering coefficients from any direction to the Ω_v direction.

$$W_M(\Delta l_i,\Omega_s \rightarrow \Omega_v) = W_M(\Delta l_i,\Omega_s) \cdot \frac{\exp[-G(j,\Omega_v) \cdot u_f(i) \cdot \Delta s_i(\Omega_v)] \cdot \int_{4\pi} \int_{2\pi} |\Omega_s \cdot \Omega_f| \cdot \frac{g_f(j,\Omega_f)}{2\pi} \cdot f(j,\Omega_f,\Omega_s \rightarrow \Omega_v) \cdot \Delta\Omega_v \cdot d\Omega_f \cdot d\Omega_s}{\int_{4\pi} \exp[-G(j,\Omega_v) \cdot u_f(i) \cdot \Delta s_i(\Omega_v)] \cdot \int_{4\pi} \int_{2\pi} |\Omega_s \cdot \Omega_f| \cdot \frac{g_f(j,\Omega_f)}{2\pi} \cdot f(j,\Omega_f,\Omega_s \rightarrow \Omega_v) \cdot d\Omega_f \cdot d\Omega_s \cdot d\Omega_v}$$

Using the relation $G(j,\Omega_s) = -\ln[T(j,\Omega_s)]$ the discretized form of $W_M(\Delta l_i,\Omega_s \rightarrow \Omega_v)$ is

$$W_M(\Delta l_i,\Omega_s \rightarrow \Omega_v) = W_M(\Delta l_i,\Omega_s) \cdot \frac{T(\Delta s_i,\Omega_v) \cdot \left\{\sum_{s=1}^{N} T(j,\Omega_s,\Omega_v) \cdot \ln[T(j,\Omega_s)] \cdot \Delta\Omega_s\right\} \cdot \Delta\Omega_v}{\sum_{v=1}^{N} T(\Delta s_i,\Omega_v) \cdot \left\{\sum_{s=1}^{N} T(j,\Omega_s,\Omega_v) \cdot \ln[T(j,\Omega_s)] \cdot \Delta\Omega_s\right\} \cdot \Delta\Omega_v}.$$

The terms $TG(j,\Omega_v) = \sum_{s=1}^{N} T(j,\Omega_s,\Omega_v) \cdot \ln[T(j,\Omega_s] \cdot \Delta\Omega_s$ are precomputed.

With lambertian leaves without specular components, we have $TG(j,\Omega_v) = \omega_d \cdot G(j,\Omega_v) = -\omega_d \cdot \ln[T(j,\Omega_v)]$. Thus,

$$W_M(\Delta l_i,\Omega_s\rightarrow\Omega_v) = W_M(\Delta l_i,\Omega_s) \cdot \frac{\exp[-G(j,\Omega_v)\cdot u_f(i)\cdot \Delta s_i(\Omega_v)]\cdot G(j,\Omega_v)\cdot \Delta\Omega_v)}{\sum_{v=1}^{N}\exp[-G(j,\Omega_v)\cdot u_f(i)\Delta s_i(\Omega_v)]\cdot G(j,\Omega_v)\cdot \Delta\Omega_v}$$

$$= W_M(\Delta l_i,\Omega_s)\cdot\frac{T(\Delta s_i,\Omega_v)\cdot\ln[T(j,\Omega_v)]\cdot\Delta\Omega_v}{\sum_{v=1}^{N}T(\Delta s_i,\Omega_v)\cdot\ln[T(j,\Omega_v)]\cdot\Delta\Omega_v}.$$

Similar considerations lead to the computaton of the expressions of $W_{sM},(\Delta l_i\Omega_s\rightarrow\Omega_v)$ source vectors. In order to avoid using a computational expensive numerical scheme for higher-order diffuse reflection, we assume that

$$\sum_{v=1}^{N}(T\Delta s_i,\Omega_v)\cdot\left\{\sum_{s=1}^{N}T(j,\Omega_s,\Omega_v)\cdot\ln[T(j,\Omega_s)]\cdot\Delta\Omega_s\right\}\cdot\Delta\Omega_v \approx \langle T_i\rangle\cdot\sum_{v=1}^{N}\sum_{s=1}^{N}T(j,\Omega_s,\Omega_v)\cdot\ln[T(j,\Omega_s)]\cdot\Delta\Omega_s\cdot\Delta\Omega_v.$$

So, we have

$$W_{sM}(\Delta l_i,\Omega_s\rightarrow\Omega_v) = \frac{T(\Delta s_i,\Omega_v)}{\langle T_i\rangle}\cdot s_M(j,\Omega_v)\cdot W_{sM}(\Delta l_i,\Omega_s)$$

with

$$s_M(j,\Omega_v) = \frac{\sum_{s=1}^{N}T_s(j,\Omega_s,\Omega_v)\cdot\ln[T(j,\Omega_s)]\cdot\Delta\Omega_s\cdot\Delta\Omega_v}{\sum_{v=1}^{N}\left\{\sum_{s=1}^{N}T_s(j,\Omega_s,\Omega_v)\cdot\ln[T(j,\Omega_s)]\cdot\Delta\Omega_s\right\}\cdot\Delta\Omega_v}.$$

The mean coefficients $s_M(j,\Omega_v)$ depend only on the scattering direction and on the cell type; they are precomputed values.

It results that the nonfoliar multiple-scattering source vectors are approximated by

$$W_{nf,M}(\Delta l_i,\Omega_s\rightarrow\Omega_v) = nf_{\text{in}}(\Omega_s)\cdot\frac{\omega_{sj}}{\omega_j}\cdot\frac{T(\Delta s_i,\Omega_v)}{\langle T_i\rangle}\cdot s_M(j,\Omega_v)\cdot W_{sM}(\Delta l_i,\Omega_s).$$

This equation satisfies the conservation of nonfoliar energy for each incident source vector $W(0,\Omega_s)$, that is,

$$\sum_{v=1}^{N}W_{nf,M}(\Delta l_i,\Omega_s\rightarrow\Omega_v) = nf_{\text{in}}(\Omega_s)\cdot\frac{\omega_{sj}}{\omega_j}\cdot W_{sM}(\Delta l_i,\Omega_s), \text{ if } T(\Delta s_i,\Omega_v)\approx\langle T_i\rangle.$$

Otherwise, this condition may not be satisfied. Thus, this equation is a first-order approximation only. However, the large number of incident vector sources on any cell leads to a large number of different middle points (M_s), which ensures that this condition tends to be verified when we consider all the incident source vectors.

Therefore, the multiple-scattering source vector that escapes cell i along (Ω_v) is

$$[W_M(\Delta l_i,\Omega_s\rightarrow\Omega_v),W_{nf,M}(\Delta l_i,\Omega_s\rightarrow\Omega_v),0],$$

where

$$W_M(\Delta l_i,\Omega_s\rightarrow\Omega_v) = W_{sM}(\Delta l_i,\Omega_s\rightarrow\Omega_v) + W_{dM}(\Delta l_i,\Omega_s\rightarrow\Omega_v).$$